Project Number: MQP DNA SHA1

VISIBLE LIGHT RESPONSIVE PHOTOCATALYTIC FUEL CELL FOR SIMULTANEOUS WASTEWATER TREATMENT AND ELECTRICITY GENERATION

A Major Qualifying Project Report:

Submitted to the Faculty of

WORCESTER POLYTECHNIC INSTITUTE

In partial fulfillment of the requirements for the

Degree of Bachelor of Science in Chemical Engineering

by

Ankush Yuvraj Patil

April 30, 2014

Approved by:

Prof. Aaron Deskins, Project Advisor

Prof. Bai Jing, Site Advisor

Abstract

Photocatalytic fuel cells (PFCs) use light as a catalyst to degrade organic molecules in wastewater, while simultaneously producing electricity. The goal of this project was to increase the efficiency of the photoanode by optimizing the fabrication process of a bismuth-doped Fluoro-doped Tin Oxide (FTO)/TiO_2 electrode. The process independent variables altered were the deposition method and number of layers of $Bi[VO_4]_3$ on the electrode's surface, photo-deposition of cobalt, and the reaction time for growing the ZnO nanotubes.

The optimized fabrication process comprised of a 3-hour reaction time for growing ZnO nanotubes, doping it with 6 layers of $Bi[VO_4]_3$ using the spin coating technique at 2000 RPM for 35 seconds, then depositing cobalt onto the surface by photo-deposition for 10 minutes. 1 layer of $Bi[VO_4]_3$ on the FTO/TiO_2 electrode resulted in an increase in current density yield by a factor of 5.83, from 0.129 mA/cm^2 to 0.752 mA/cm^2. The 6 layers of $Bi[VO_4]_3$ doping further increased the current density output by a factor of 2.14, to 1.46 mA/cm^2. Total photovoltaic efficiency was increased by a factor of 11.3. Bismuth proved to be an effective doping chemical with a promising future.

Acknowledgements

This project was a collaboration of many individuals who I had my greatest pleasure to work with. This was my first experience going abroad and completing a project and I would say it was a successful experience thanks to a few people that I would like to thank. Firstly, my WPI advisor, Professor Aaron Deskins, has been a lot of help all along the way. I would like to thank him for keeping in touch me and with my progress in the project while I was in Shanghai. I would also like to thank him for directing me in the right direction whenever I had questions or doubts regarding my report. He has also been very patient with me as I worked on completing this report. I would also like to thank my Shanghai Jiao Tong University's on-site advisor, Assistant Professor Bai Jing, who I had the pleasure to work with for 2 months. He helped me achieve the goals of this project and furthered my understanding of photocatalytic fuel cells and how I, as a Chemical Engineer, can play an important role in the development of this technology. He answered all my questions regarding the project and helped me with any living problems I came across during my time in Shanghai. I would like to thank WPI's Chemical Engineering Department and IGSD, and SJTU's Environmental Department for giving me this opportunity to travel to China for this unique experience.

Table of Contents

Table of Figures

Table of Tables

1 Introduction

The global demand for energy has now reached higher than ever before and continues to increase. World population is still on the rise and urbanization is occurring at a faster rate all over the world. Taking these trends into account, it is possible that the world could reach an energy crisis. Certain parts of the world, especially India and China, are already witnessing some sort of an energy crisis, where the demand for energy is greater than the supply. For now, non-renewable resources, such as oil, coal, and gas, are the major sources used to produce energy, but these sources are slowly depleting. Renewable energy, which consists of hydropower, wind power, solar power, etc., accounted for nearly 13% of the total energy production in 2010 (Ross, 2010). According to statistics from Energy Information Administration, in 2010 the world demanded about 154 trillion kWh, and it is estimated that by the year 2040 that number will have increased by 60% (Doman, 2013). Therefore, finding new sources of energy has become more important than ever before.

Other than an energy crisis, the world is also challenged with growing waste, mostly constituting of wastewater. According to Pacific Institute, the world discharges about 2 million tons of solid waste daily into water bodies. This is leading to increased water pollution in many areas around the world (Ross, 2010). Wastewater generally originates from sewage (human waste and surface runoff), agriculture, and various industries. While some of it is treated through a wastewater treatment facility and reused, most is dumped back into a body of water creating problems for the aquatic ecosystem. Untreated wastewater has significant impacts

on human health, the ecosystem, and eventually the economy. It is estimated that 1.8 billion people in Asia do not have access to clean water. Waterborne diseases are the number one cause for child death. Untreated wastewater has also led to endangerment of many species and disruption in freshwater ecosystems. These disruptions have cost the world economy a total of US$ 75 billion in goods and services (Ross, 2010). Therefore treating wastewater is important for the future of every country. Wastewater treatment facilities help get rid of organic waste, heavy metals, and toxins in the wastewater. Organic waste contains organic molecules, whose chemical bonds can be used to generate electricity. Energy contained within these chemical bonds is the source of electricity. It is estimated that the total amount of energy contained in the chemical bonds of organic wastes are 36 trillion kWh (Liu, Li, Zhou, et.al, 2011). It has, therefore, become important to come up with a technological solution to extract this available energy, instead of dumping it into water bodies and creating more pollution. One such technological solution is the photocatalytic fuel cell (PFC).

A PFC is capable of converting the energy stored in chemical bonds in organic molecules into electricity, while simultaneously removing organic waste. This tackles both the energy crisis and the water pollution problems. A fuel cell is any device that converts the energy stored in chemical bonds into electricity. Every fuel cell consists of an anode (a negative side), a cathode (a positive side), and an electrolyte that allows the passing of charges between the negative and positive sides. Fuel cells will operate, as long as there is a continuous source of fuel and oxygen. In a photocatalytic fuel cell, light is used as a catalyst to activate the

breakdown of organic molecules at the anode, or photoanode, and thus leads to the transfer of electrons. The lack of knowledge and the inefficiency of PFCs have restricted its growth and use in the energy and industrial sectors. A PFC built on a titania-based photoanode, has been widely tested and has proved effective, but this anode requires the use of UV light for activation. For a more efficient process, a photoanode that relies on solar light would be ideal and serve as a real advantage. Achieving an efficient process with a visual light, or solar light, responsive PFC would be a big step forward in creating a greener world for the future. Along with the "green" initiative, the development of this technology could, potentially, allow third world countries access to cleaner water as well as electricity.

1.1 Project Goals

The goal of this project is to fabricate electrodes that will be used as photoanodes in PFCs and to identify a doping chemical to enhance its performance. Once the doping chemical is identified, this project will determine the fabrication process that would greatly optimize the photoanode's responsiveness to visible light. The photoanode will be characterized using techniques such as photoelectrochemical (PEC) tests, scanning electron microscopy (SEM), and x-ray diffraction (XRD) in order to determine its physical and electrochemical properties.

1.2 Report Organization

The report begins by introducing relevant background information required to understand the importance of this technology, its history and progression through the years, its major characteristics, and the tools required to understand the findings presented in this paper. After the background information has been

provided, the report will specify the detailed objectives of this report and how they will be met. The design and methodology of the experiment follows the project objectives, specifying exactly how the objectives were met through detailed procedures. Following the methodology section is the results and discussion section, where results achieved from the experiment will be presented, analyzed, and discussed. This will include an analysis of each experimental process that yielded results, reasons explaining the validity of the results, and, if appropriate, a discussion comparing the experimental values to known values from other works. Then, follows a conclusion section, summarizing the results and discussing which project objectives were met. The final section of this report will provide recommendations for future repetitions of this experiment. This section also discusses possible directions for future work to further optimize the photoanodes efficiency.

2 Background

Before developing and optimizing a new photoanode through different characterization methods, in depth research has been conducted into the relevant previous research. A thorough understanding of the importance, historical development, design, and function of a PFC is essential to forming a proper project approach and methodology. The background research presents the importance, design, and functions of fuel cells, in particular PFCs, and introduces the theory behind different characterization techniques that will be used in developing and optimizing a new photoanode.

2.1 The Importance of Treating Wastewater

Wastewater is defined as any effluent generated from a commercial, residential, agricultural, or industrial area that contains dissolved or suspended matter, such as organic and inorganic matter. Wastewater is either treated and reused or released into a body of water, such as lakes, rivers, and seas. The United Nations Environment Program (UNEP) estimated that nearly 90% of all wastewater in developing countries is released untreated into bodies of water (Nakamura). Continuous untreated wastewater discharge into water bodies severely disrupts aquatic life by creating dead zones. A dead zone represents an area within a water body where the oxygen content in the water is scarce and therefore no aquatic life is able to survive. These dead zones originate because microorganisms use the organic matter in wastewater and dissolved oxygen from the body of water, where the effluent is discharged, to produce energy, which is their "food". As more organics are released into a body of water, the microorganisms use more oxygen to produce

energy, and therefore less oxygen is available for the aquatic ecosystem in that area. An effluent's biological oxygen demand (BOD) can quantify the amount the degree of pollution of wastewater and also aid in determining effectiveness of wastewater treatment facilities. BOD is defined as the amount of dissolved oxygen required for microorganisms to convert the organics in wastewater into energy. Therefore, the higher the BOD for a sample of wastewater the more organic material is present and, therefore, the more polluted that stream. Releasing a high BOD rated wastewater into bodies of water, greatly affects regions whose fisheries are major contributors to that economy. This also affects the livelihoods of people who depend on aquatic life as their main source of food and business. Along with a region's economy, the people's health is also at risk as deaths form waterborne diseases, such as diarrhea, are the most common among children in the third world countries. Treating wastewater has huge benefits for a population as they get access to clean water and an improved environment.

2.1.1 Current Methods of Wastewater Treatment

Wastewater is generally treated through five different stages; preliminary, primary, secondary, tertiary, and disinfection. Wastewater treatment methods can be classified into three different classes; mechanical operation, chemical operation, and biological operation. Each operation uses their respective force to remove pollutants; physical separation in mechanical operation, chemical reactions in a chemical unit process, and biological activities in a biological unit process.

The preliminary stage in a wastewater treatment facility is to screen large solids that are suspended in wastewater. Along with screening, breaking down large

materials to finer particles, also known as communition, is carried out. The wastewater then flows through grit removal chambers, where fine particles are removed. The preliminary step is a combination of different mechanical operations and is an important step to protect the downstream equipment, such as pipes, vessels, and pumps, from suspended solids. Wastewater treated through the preliminary stage moves on to the primary stage.

The primary stage removes pollutants that settle at the bottom of the tank through sedimentation and removes pollutants that float to the top of the tank by screening or skimming. This stage removes 25-50% of the organics, 50-70% of the suspended solids, and 65% of the oil and grease ("Wastewater treatment and," 1992). The primary step is also consists of mechanical operations. The wastewater then moves on to the secondary stage.

The main purpose of the secondary stage is to treat the dissolved pollutants, mainly organics, as the previous stages were not able to do so using physical separation techniques. The effluent is treated in biological reactors where a combination of microorganisms and aeration is used to decompose organic compounds. The effluent then moves on to the tertiary stage.

The tertiary stage, or advanced treatment, is only used when certain pollutants cannot be removed from the secondary stage, such as heavy metals, nitrogen, and phosphorus. The tertiary stage consists primarily of chemical operations ("Wastewater treatment and," 1992). After the effluent is treated through the stages, it is disinfected with the use of chlorine. Figure 1, below, shows a

general process flow diagram of a wastewater treatment plant. The diagram below does not include the tertiary stage.

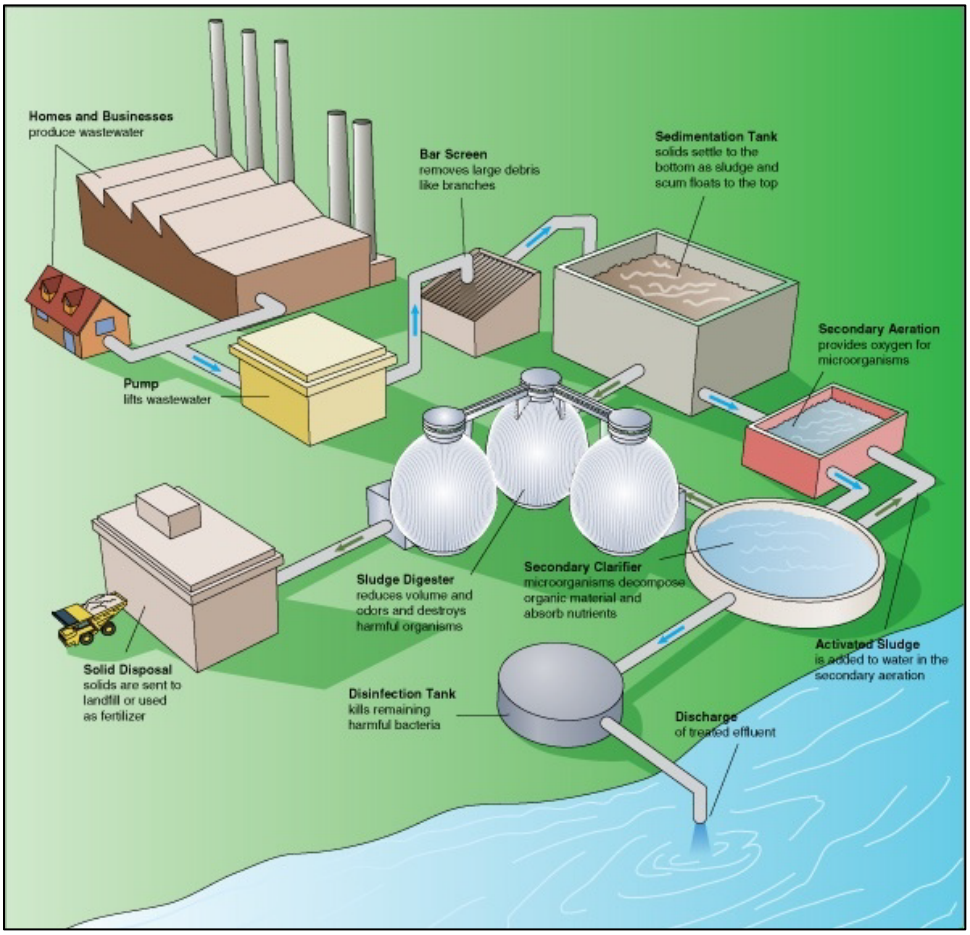

Figure 1: Process flow diagram of a typical wastewater treatment plant
http://upload.wikimedia.org/wikipedia/commons/2/2a/Steps_in_a_typical_wastewater_treatment_process.png

Figure 1, shows how a wastewater treatment plant treats wastewater form households and businesses. The diagram shows an additional process, known as sludge digester, which is responsible for storing solids, oils, and other materials that were screen and removed from the water and treat them so they can be disposed of in a landfill.

However, not all wastewater treatment facilities around the world are able to treat their wastewater through the first four stages, but they all end the process

with disinfection. According to UNESCO, 86% of the collected wastewater in North America is treated to the secondary level, in Europe it is 63%, 16% in Asia, 5% in Latin America, and less than 0.5% in Africa (Zandaryaa, 2011). Most of the developing countries around the world are not able to afford the equipment required to treat their wastewater, and therefore they end dumping the effluents into water bodies. It has become important to develop inexpensive technology that is effective in treating wastewater.

2.2 Fuel Cell Theory

A fuel cell is any device that is capable of transferring electrons from an anode to a cathode to produce a current with the help of electrochemical reactions. An electrolyte separates the two electrodes and allows the passing of positive ions to the cathode and negative ions to the anode. The A basic example of a fuel cell is shown below in Figure 2.

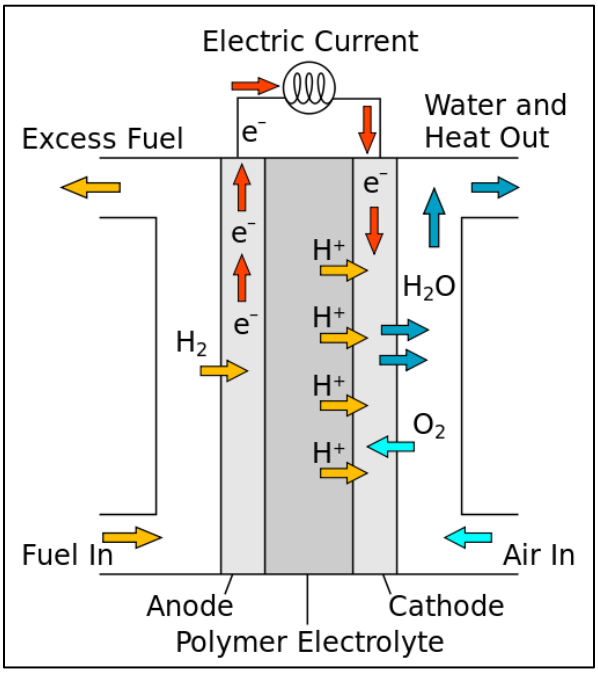

Figure 2: Schematic of a basic fuel cell
http://upload.wikimedia.org/wikipedia/commons/9/9b/PEM_fuel_cell.svg

In this example, hydrogen is used as the basic fuel. Oxygen is also necessary to complete the reaction and form products. A hydrogen source can be provided to a fuel cell in either its pure form, H_2, or in molecules like methane, CH_4. Air is usually used as the oxygen source. A general fuel cell is comprised of two chambers; an anodic chamber, where the anode is placed, and the cathodic chamber, where the cathode is placed. The two chambers are separated by an electrolyte, which can be a liquid solution or a solid membrane. The electrodes can be made up of various types of materials, based on how efficiently it traps and transfers electrons and which catalysts are necessary to initiate the reaction. The materials for the anode are chosen according to its efficiency in stripping off electrons form hydrogen, acting as catalysts. Once the anode strips electrons off of the hydrogen, now a cation, hydrogen travels across the electrolyte and into the cathodic chamber. On the other hand, the electrons stripped away from the hydrogen, travel from the anode through an electrical circuit and into the cathode. The oxygen supplied to the cathodic chamber, combines with the hydrogen ions and electrons to form water as a product. The reaction that takes place in the fuel cell is known as an oxidation-reduction reaction. Oxidation is the process of removing electrons, thus decreasing the ionic charge on a molecule, while reduction is the process of adding electrons, thus increasing the ionic charge of a molecule. In Figure 2, oxidation occurs at the anodic chamber, represented by $H_2 \rightarrow 2H^+ + 2e^-$. The reduction reaction occurs at the cathodic chamber, represented by $\frac{1}{2}O_2 + 2H^+ + 2e^- \rightarrow H_2O$. The overall oxidation-reduction reaction is represented by $H_2 + \frac{1}{2}O_2 \rightarrow H_2O$. The primary difference in fuel cells lies in the type of electrolyte between the two chambers and

in the material of the electrodes. There are many types of fuel cells that have proved effective, but they each have their drawbacks.

2.2.1 Types of Fuel Cells

The different types of fuel cells along with their characteristics are summarized in Table 1, below. Some important characteristics help determine the application and benefits of different fuel cells. A catalyst required to initiate the oxidation of a molecule plays an important role in a fuel cells efficiency and power output. A catalyst is generally a mixed into the material of the anode. It is important to understand that the power output of a fuel cell is directly correlated with the size of the fuel cell, while the efficiency is related to the completion of the oxidation-reduction reactions within the fuel cell, which is dependent on the catalyst, electrode materials, and electrolyte. The disadvantages to each fuel cell are also noted. From Table 1, it is evident that the only types of fuel cells that tackle wastewater problem, while simultaneously generating electricity, are the microbial fuel cells (MFCs) and the photocatalytic fuel cells, as they decompose organic matter.

Table 1: Characteristics of different fuel cells and their major disadvantages ("Types of fuel," 2014)

Type of Fuel Cell	Electrolyte Material	Catalyst for Reactions	Fuel Type	Operating Temperature (°C)	Efficiency	Power Output (KW)	Disadvantages
Alkaline	KOH in Water	Platinum	Pure H_2	150 – 200	60%	0.3 - 5	• Platinum is very expensive • Requires pure hydrogen for fuel • Easily poisoned by CO_2
Phosphoric Acid	Liquid phosphoric acid	Platinum	Hydrocarbons, Biogas	150 – 200	40% - 80%	200 – 11,000	• Platinum is very expensive • Corrodes over time
Molten Carbonate	$NaCO_3$ or KCO_3 in a $LiAlO_2$ matrix	Nickel	Hydrocarbons, Carbon Oxides	650	60% - 80%	2,000 – 100,000	• Operating temperatures are too high • Necessary to feed CO_2 to fuel cell
Solid Oxide	Solid ceramic (YSZ)	Nickel	Hydrocarbons	1000	50% - 80%	100	• Operating temperatures are too high • Solid ceramic electrolyte can crack
Proton Exchange Membrane	Solid polymer membrane	Platinum	H_2, MeOH, reformed fuels	80 – 110	40%-50%	50 – 250	• Platinum is very expensive • Purified fuels must be used
Direct Methanol	Solid polymer membrane	Platinum	Pure MeOH	50 – 120	<40%	0.25 – 5	• Platinum is very expensive • Pure MeOH fuel required
Microbial	Solid polymer membrane	Microorganism	Any organic matter	20 – 40	<50%	0.00188/ m^2	• Very slow process • Require large units for high power outputs
Photocatalytic	PEMs	UV/Visible Light	Any organic matter	20-40	50-60%	Size dependent	• New research topic • Not industrially applicable

2.3 Microbial Fuel Cells (MFCs)

A MFC uses microorganisms as catalysts to breakdown hydrogen-rich organic molecules, with the help of oxidation-reduction reactions, and generate a current through an external electrical circuit. A MFC can be considered as a bioreactor or, in reference to Section 2.1.1 in this report, the secondary stage in a wastewater treatment facility, meaning it's able to remove organic pollutants from wastewater. A diagram of a basic MFC treating wastewater is provided in Figure 3, below.

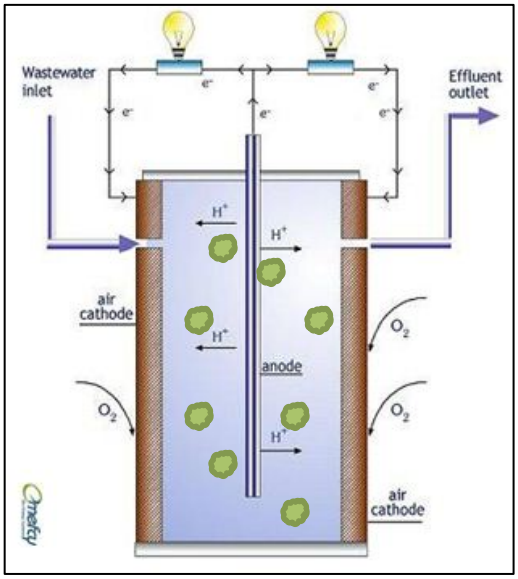

Figure 3: MFC process for converting wastewater to electricity
http://upload.wikimedia.org/wikipedia/commons/2/2f/Emefcy-MFC.JPG

The green spots in the cell represent the microorganisms. Wastewater can contain numerous types of organic molecules that can act as a fuel source for a MFC. Below, is a set of oxidation-reduction reactions that would take place if glucose were present in the wastewater stream.

Oxidation: $C_6H_{12}O_6 + 6H_20 \xrightarrow{microorganisms} 6CO_2 + 24H^+ + 24e^-$ (1)

Reduction: $6O_2 + 24H^+ + 24e^- \rightarrow 12H_2O$ (2)

Overall: $C_6H_{12}O_6 + 6H_20 \xrightarrow{microorganisms} 6CO_2 + 12H_2O$ (3)

As seen from equation (3), the products of the overall reaction are 6 moles of carbon dioxide and 12 moles of water for every mole of glucose decomposed. The selective membrane or electrolyte only allows H^+ ions to flow towards the cathode. This type of membrane is called a proton exchange membrane (PEM), as it solely allows protons, such as H^+, to pass through it. In Figure 3, the blue substance around the anode represents the PEM. It is important to keep the anodic chamber anaerobic, to keep the oxygen away from the microbes. If oxygen were to pass through to the anodic chamber, then the organic matter would still breakdown, but it would not produce any electrons. It is also important to know that the interaction between the microorganisms and the anode plays a crucial role in generating electricity. The microorganisms decompose the organic molecules and transfer the electrons to the anode, which in turn goes through an external circuit to the cathode to produce electricity.

2.3.1 Performance of MFCs

The performance rating of a MFC depends on its activation polarization, concentration polarization, its ohmic losses, and. Activation polarization is defined as the activation energy required for the redox reaction to occur to result in electron flow. The reaction kinetics of the decomposition of organic molecules by microbes, the transfer of electrons from the microbes to the anode, and the material and structure of both the anode and cathode play an important role in determining the activation polarization. Activation polarization of a cell can be improved by altering operating conditions, such as type of microorganisms, concentration of organics in

wastewater, pH, temperature, and reactor design. Another important factor in improving activation polarization is the type of electrode material used. Electrodes constructed from or coated by platinum (Pt) perform better when compared to graphite or carbon-cloth electrodes. Concentration polarization is defined as the inability to maintain an initial microorganism in the anodic chamber or oxygen concentration in the cathodic chamber. MFCs aim at lowering concentration potentials by increasing mass transfer within a chamber, like stirring and bubbling. Furthermore, ohmic losses are the losses in electric potential due to inefficiency of electron transfer. Improving the conducting wire material, decreasing the surface area of PEMs, and reducing the distance between the electrodes can reduce the ohmic losses (Du, Li & Gu, 2007).

A MFC's actual cell potential is used to rate its performance. (Appleby and Foulkes, 1989) came up with an equation to represent a MFCs cell potential,

$$V_{Cell} = E_{Cathode} - \left|\eta_{act,c} + \eta_{conc,c}\right| - E_{Anode} - \left|\eta_{act,a} + \eta_{conc,a}\right| - iR_i \quad (4)$$

where $\eta_{act,c}$ and $\eta_{act,a}$ represent the cell's activation polarization at the cathode and anode, respectively, and the $\eta_{conc,c}$ and $\eta_{conc,a}$ represent the cell's concentration polarization at the cathode and anode, respectively. The iR_i is the term used to represent ohmic losses due to the resistance of flow of electrons and ions between cathodes and chambers, respectively, where i is the current flow and R_i is the total resistance in the fuel cell (Du, Li & Gu, 2007).

However, in spite improving different conditions to reduce activation and concentration polarization and ohmic resistance, there lies a limit to a MFC's performance. The limit lies in the reaction kinetics between microorganisms and the

organic molecules and in the transfer of electrons from the microorganisms to the anode. Both these limits would be categorized as an activation polarization property. Microorganisms are relatively very slow at decomposing the organic molecule and transferring the electrons to the anode, when compared to the rest of the MFC process. These process attributes are therefore considered the rate-limiting step in the overall redox reaction. The rate limiting process can be improved by using different microorganisms that are faster at breaking down organic molecules or coating the anode with a catalyst so the transfer of electrons between microorganisms and the anode is faster. However, current technology limits the speed of this process. Despite MFC's capability to simultaneously treat wastewater and produce electricity, they prove to be highly inefficient for industrial and commercial use, as these are fast growing sectors and require an equally efficient technology. One possible solution is the use of photocatalytic fuel cells.

2.4 Photocatalytic Fuel Cells (PFCs)

PFCs use light, such as ultraviolet (UV) light or visible light, as a catalyst to initiate the redox reaction. The main focus of this report will be on visible light PFCs. PFCs maintain the same properties of MFCs, in terms of structure, function, and process, but differ in the initiation of the reaction, or in one aspect of the activation polarization. The activation of the reaction is known as semiconductor photocatalysis. The most common type of visible light PFCs use a TiO_2 based anode and a platinum based cathode. The electrolyte material, however, varies depending on its application. Most common electrolytes include potassium chloride (KCl) and sodium sulfate (Na_2SO_4).

2.4.1 Semiconductor Photocatalysis

Semiconductor photocatalysis is the process that initiates and sustains the redox reaction in a PFC. The electron configurations in a semiconductor is unique, as it has a filled valence band and an empty conduction band, which allows light to act as a catalyst and create electron-hole pairs. A valence band is defined as the outermost ring of electrons in an atom, but these electrons are tightly bound to the nucleus and not allowed to move freely (McGraw-Hill Dictionary, 2003). A conduction band is defined as outermost orbital of an atom to which electrons can move around freely (The American Heritage® Science Dictionary, 2005). These two bands are known as the energy bands and the space between them is the band gap. This theory is important as it helps distinguish between insulators, conductors, and semiconductors, as seen in Figure 4.

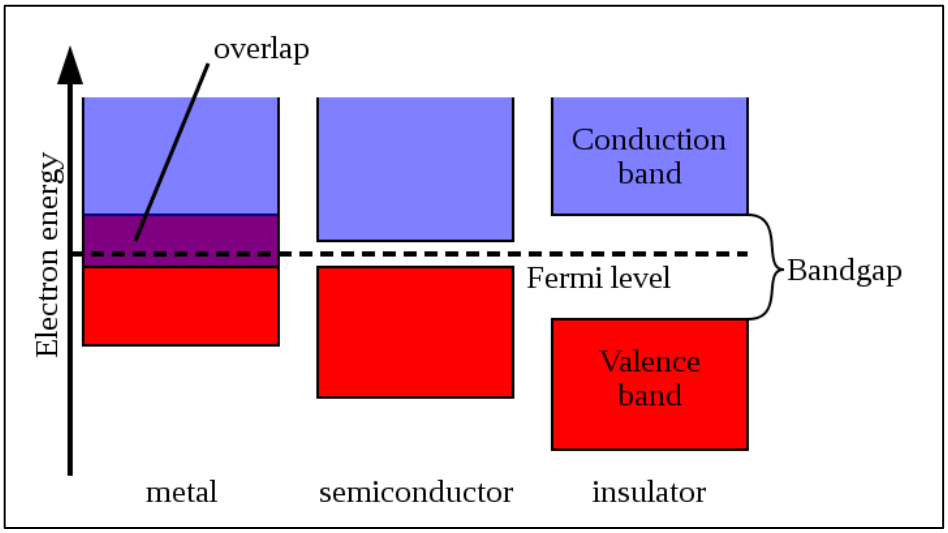

Figure 4: Difference between Insulators, Semiconductors, and Conductors
http://upload.wikimedia.org/wikipedia/commons/c/c7/Isolator-metal.svg

Figure 4, shows how the valence bands and conductions bands are placed within insulators, conductors or metals, and semiconductors. When the energy gap, band gap, is too large, then electrons cannot be transferred form the valence band to

the conduction band. These materials are classified as insulators. When no band gap exists, the valence and conduction band overlap, and the material is classified as a conductor. A semiconductor is known to have an energy gap that is small enough to be overcome by sources of energy such as heat or light (Nave, 2014). When there is a large enough energy source for a semiconductor, then electrons from the valence band will move to the conduction band, leaving behind holes in the valence band. The holes left behind are powerful oxidizers and assist in breaking down organic molecules. Figure 5, below, shows the band gaps for various semiconductors. The top and bottom boundary of the grey shaded area represents the auto redox voltage for the reduction and oxidation of water, respectively. Auto redox occurs when the voltage being supplied initiates a redox reaction, rather than energy from light. This can happen when the PFC is receiving a voltage from an external source. The auto reduction voltage for water is about 0V and for auto oxidation it is about 1.2V. When analyzing results, it is important to keep the analysis in this boundary, 0V – 1.2V. When selecting the appropriate semiconductor to use for our application, it is important to select one that covers the grey shaded region while keeping the energy gap as small as possible. Therefore, from Figure 5, we can eliminate all the semiconductors that do not cover the grey shaded region, which are GaAs, GaP, Fe_2O_3, WO_3, and SnO_3. Furthermore, CdSe and CdS are considered to be unstable under photocatalysis (Adeli, 2013). Available semiconductors to use as the photoanode are ZnO, TiO_2, and SiC. In this report; we will be using TiO_2 as our photoanode due to its high efficiency, low cost, and stability (Liu, Li, Zhou, et.al., 2011).

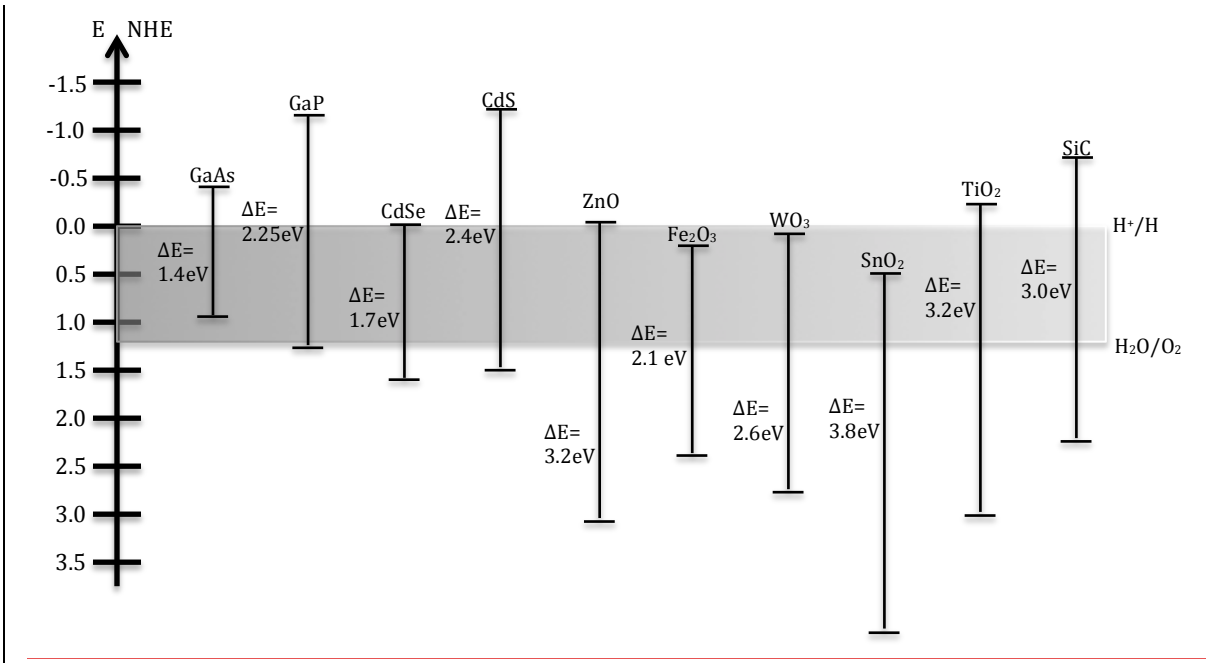

Figure 5: Energy gaps for various semiconductors

2.4.2 Optimizing the Performance of Photoanodes

Semiconductors have a crystal lattice structure, meaning their atoms are closely packed together and the valence electrons are not free to move around. Therefore, some amount of energy is required to move these electrons from the valence band into the conduction band. However, the energy gap of any semiconductor can be reduced through using doping techniques. Doping a semiconductor with certain elements allows impurities to be added to that crystalline structure. These impurities help improve the conductivity of the semiconductor by either creating additional electrons or additional holes, depending on the element that is used for doping. Figure 6, below, show the effects of doping a semiconductor with specific elements to create impurities.

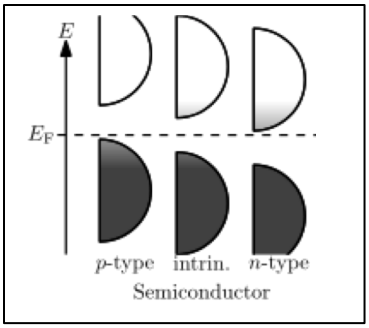

Figure 6: Band gaps in p-type and n-type semiconductors
http://upload.wikimedia.org/wikipedia/commons/9/9d/Band_filling_diagram.svg

As seen in Figure 6, the Fermi level is constant for all three types of conductors, intrinsic, n-type, and p-type, but the valence band or conduction band move closer to the Fermi level. In p-type semiconductors, the valence band is closer to the Fermi level. This is also known as the conduction band's "acceptor level". The energy required to move electrons from the valence band to the conduction band decrease as the conduction band more readily accepts electrons due to the impurity. On the other hand, in n-type semiconductors the conduction band is closer to the Fermi level, which is also known as the valence band's "donor level". For n-type semiconductors, the energy required to move electrons from the valence band to the conduction band decreases as the valence band more readily gives up electrons due to the impurity. The doping chemical used to create impurity for p-type semiconductors are any of the group 13 elements, where as to create impurity for n-type semiconductors, any of the group 15 elements can be used. Doping a semiconductor with a group 13 element, such as Gallium, results in the formation of "holes" or a lack of electrons. These holes act as impurities in the semiconductor that allow an easier transfer of electrons between the two bands. Doping a semiconductor with a group 15 element, such as Phosphorus, results in extra

electrons in the valence band resulting in an easier transfer to the conduction band. Figure 7, below gives a clear picture of the atomic views of the three types of semiconductors. An intrinsic semiconductor is one that has no impurities.

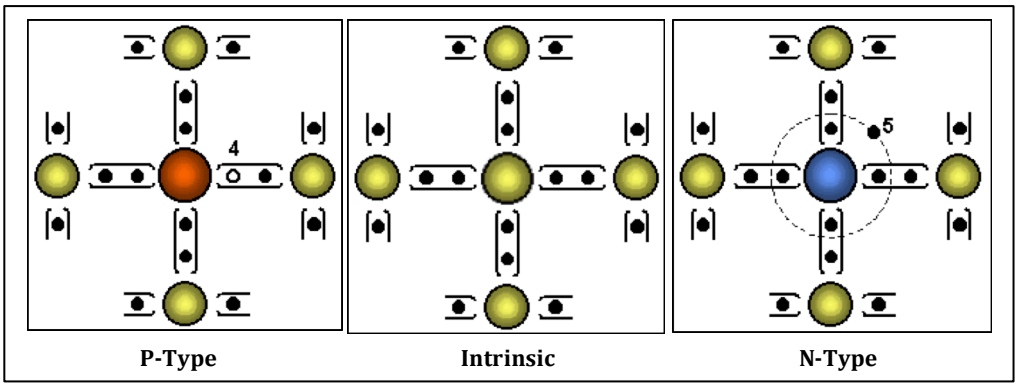

Figure 7: Atomic structure of intrinsic and doped semiconductors
http://upload.wikimedia.org/wikipedia/commons/c/cf/Semiconductor_tipo_p.png
http://upload.wikimedia.org/wikipedia/commons/f/ff/Semiconductor_tipo_n.png

In Figure 7, the hole in the p-type semiconductor is represented with the number 4 and number 5 represents the extra electron for the n-type. This report focuses on using intrinsic TiO_2 as the base semiconductor and doping it with chemicals to improve its efficiency as a photoanode.

2.4.3 Progress of TiO_2 as a Photoanode

Since the early 1900s, TiO2 was considered as a stable compound in the dark and an erratic compound when it came to contact with light. It was reported that TiO_2 was able to bleach dyes or degrade paint on houses when it came in contact with light. It wasn't until 1972 that Fujishima and Honda determined the photocatalytic water-splitting properties of crystalline TiO_2 in 1972. They determined that TiO_2 could degrade water when it is illuminated with UV light. During this process the reaction produced oxygen and hydrogen molecules while

producing electricity along an external circuit. Below is set of redox reactions that show how TiO_2 was used in water splitting.

At TiO_2 electrode: $TiO_2 + hv \rightarrow h^+ + e^-$ (5)

Oxidation: $H_2O + 4h^+ \rightarrow O_2 + 4H^+$ (6)

Reduction: $2H^+ + 2e^- \rightarrow H_2$ (7)

Reaction 5 shows how the electron-hole pair is created by the activation of the TiO_2 anode by UV light (hv). The holes created in the valence band are able to oxidize water and create hydrogen ions and electrons. These electrons pass through an external circuit and return to the cathode to combine with the diffused hydrogen ions to form hydrogen molecules, as represented by reaction 6 and 7, respectively. The efficiency of this process was very low, reaching maximum of 10-11% by the end of the decade (Hashimoto, Irie & Fujishima, 2005). However, since this discovery, there has been an upsurge in research and development to more effectively use TiO_2 as a photoanode in PFCs.

In the 1980s, the application of TiO_2 diverted form crystalline photocatalysis to powdered photocatalysis. This approach had high hopes as the surface area of available for UV activation for TiO_2 increased significantly. However, despite the increase in surface area, the efficiency was still very low. Kawai and Sakata examined the reasons behind the low efficiency and found that the production sites of the H_2 and O_2 gas molecules were close enough to each other for the reaction to reverse and form water molecules, making the reaction highly inefficient. To avoid this reaction from reversing, they introduced organic molecules and a cathode, in the form of platinum, and observed an efficiency of 50%. However, despite the high

efficiency, the TiO_2 still was not attractive for industries as only UV light, which is only 3% of the solar spectrum, could activate the photoanode (Hashimoto, Irie & Fujishima, 2005). The platinum cathode was also too expensive to be used industrially. Therefore, the progress of TiO_2 as a photoanode is highly dependent on its activation by visible light. This can be achieved by doping the photoanode with an appropriate chemical to decrease its band gap.

2.5 Semiconductor Characterization Techniques

Semiconductor characterization techniques are used to better understand the quality of a semiconductor by looking at its electrical, optical, physical, and chemical attributes. Understanding how these attributes change according to process changes will help determine the most efficient photoanode and the fabrication process required to achieve that efficiency.

2.5.1 Photo-electrochemical (PEC) Test

A PEC test helps determine the photovoltaic activity of a semiconductor or photoanode. The test uses a light source to activate the photoanode, which is called the work/experimental electrode. The system also consists of a cathode, also called a counter electrode, generally platinum (Pt). Additionally, it consists of a reference electrode. All three electrodes are placed in a small, clear cell with an electrolyte. Voltage supply to the work electrode is controlled, through an external source, to generate a potential difference for electrons to flow. With the help of a electrochemical analyzer, data on photovoltaic activity can be generated in terms of time-current graphs and voltage-current graphs (Liu, Li, Zhou, et.al., 2011).

2.5.2 Scanning Electron Microscopy (SEM)

A SEM is a machine that uses electrons to generate microscopic images of an object. An electron gun fires electrons at an object under investigation and the way each electron reflects off the object helps determine its microscopic image. This technology is helpful in determining an object's texture. Using the microscopic images of a photoanode's texture, the photoanode can be physical characterized (*Scanning electron microscopy*, 2013).

2.5.3 X-Ray Diffraction (XRD)

An X-ray diffraction, or X-ray crystallography, is a method through which one can identify the atomic and molecular structure of a crystal. The machine uses beams of X-rays and shoots it at the subject and measures the diffraction beams. The angles and intensities of the diffracted X-ray beams help generate a 3-D image of the subject and more importantly it identifies the chemical make-up of the subject. This technology is helpful in determining chemical bonds of an unknown crystalline substance (Merriam-Webster Dictionary, 2009).

3 Project Approach

3.1 Project Objectives

1. Be able fabricate FTO/TiO_2 electrodes and determine the doping chemical:
    a. In order to fabricate the electrodes, Prof. Bai Jing from SJTU will provide me with the appropriate procedures and training during the first week.
    b. Prof. Bai Jing and Nick will conduct the preliminary research to determine which chemical to use as the doping chemical on the electrodes. This decision will be based on past papers from researchers. I will conduct research on various doping process that can be used.
2. Optimize the fabrication process of FTO/TiO_2 electrodes and the doping process:
    a. Once I have learned the fabrication process and selected the method for doping the electrode with the specified chemical, I will be varying many of the controlled variables in the fabrication process to optimize the photovoltaic activity of the electrode.
3. Use characterization techniques to conduct analysis on fabricated electrodes.
    a. Photo-electrochemical (PEC) test will be the primary test used to determine the efficiency of the electrode fabricated. The PEC test will be conducted on each successfully fabricated electrode for comparison.
    b. The SEM and XRD tests will only be conducted on electrodes that show high performance in the PEC test. The Environmental Engineering department will run the two tests, and I will only have access to the results.

4 Design & Methodology

The following procedures were used to design the electrodes and meet the project objectives. The preliminary part of the project requires me to prepare FTO/TiO_2 electrodes based on procedures recommended by Professor Bai Jing from Shanghai Jiao Tong University. The element, bismuth (III) or Bi^{3+}, in the form of $Bi[VO_4]_3$, was chosen as the doping chemical for this study, and is based off of a prior study conducted by Marcelo Rodrigues da Silva (Rodrigues da Silva, Lucilha & Afonso, 2013). The methodology for determining the most efficient FTO/TiO_2 doped with $Bi[VO_4]_3$ will be based on varying various process techniques for fabricating the FTO/TiO_2 and doping $Bi[VO_4]_3$ on to the electrode.

4.1 Preparation of a FTO/TiO_2 Electrode

A transparent conducting film (TCF), in particular transparent conducting oxide (TCO) glass composed of fluorine-doped tin oxide (FTO), is used as the electrode base. A TCF has one particular side that is conductive, which was determined using a voltmeter. The non-conductive side was then engraved for easier distinction. The FTO glass was then cleaned through a two-step process. The first step involved submerging the FTO glass, with the help of a plate rack, in a diluted Triton X-100 ($C_{34}H_{62}O_{11}$) solution in a beaker. This beaker was placed in an ultrasonic cleaner at room temperature for 30 minutes. The FTO glass was then rinsed with deionized (DI) water. The second step involved cleaning the FTO glass with isopropyl alcohol (C_3H_8O), and then with DI water, using the same process as done with Triton X-100. After the final rinse with DI water, a hairdryer was used to dry the electrodes.

4.1.1 Growing ZnO Nanotubes on FTO Glass

Next step was to form a zinc oxide (ZnO) nanoparticle layer on the conductive side of the FTO glass. A seed solution composed of 0.09g of zinc acetate dihydrate ($C_4H_6O_4Zn \cdot 2H_2O$) dissolved in 20mL of ethanol (C_2H_6O) was prepared. Three to four drops of the zinc acetate solution were then placed on the conductive side of the FTO glass. Using the spin coating technique, with the help of POLOS SPIN 150, the solution formed a thin, flat layer over the glass. Spin coating was carried out at 1500RPM for 20 seconds. The spin coating technique is graphically represented in Figure 8. The glass was then dried/heated on a hot plate at 150°C for around four to five minutes to evaporate the acetate and leave a solid ZnO coating. The glass was then air-cooled on a metal plate for about three minutes. The spin coating, drying/heating, and cooling steps were repeated five more times at the same parameters. However, for the last repeat the FTO glass, now FTO/ZnO electrode, was left on the hot plate at 400°C for two hours and then cooled down at room temperature. During each step, it was made sure that the conductive side of the glass was facing up. The ZnO coating on the FTO glass was now a multilayer of ZnO nanoparticles.

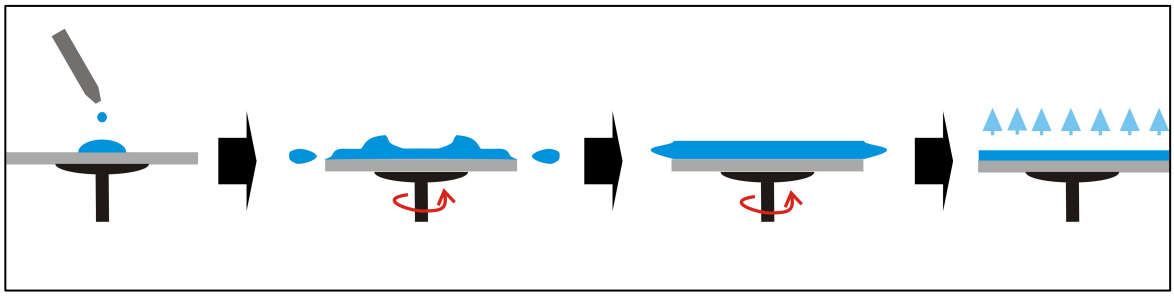

Figure 8: Spin coating technique
http://upload.wikimedia.org/wikipedia/commons/f/f3/SolGel_SpinCoating.jpg

These layers of nanoparticles were then converted to a layer of nanotubes. A gross solution was prepared, which was composed of 3.72g of zinc nitrate hexahydrate ($Zn[NO_3]_2 \cdot 6H_2O$) and 1.75g of hexamethylene tetramine ($C_9H_{12}N_4$) dissolved in 500mL of DI water, in a reagent glass bottle. Three of the FTO/ZnO electrodes were suspended in the solution using a heat and chemical resistant polyimide tape, making sure to tape the non-conductive side. The lid was placed on the bottle and the bottle was placed in an oven for three hours at 94°C. Figure 9 shows the suspended FTO/ZnO electrodes in the gross solution after three hours of heating at 94°C. The electrodes were then rinsed thoroughly with DI water and dried using a hairdryer. Using a HNO_3 dipped cotton swab, the ZnO coating was removed from the very top of the electrode, revealing the conductive FTO glass, as shown later in Figure 10. The electrodes were then placed on a hot plate, conductive side up, at 200°C for two hours. Layers of nanotubes ZnO now coated the FTO/ZnO electrodes and were ready be fabricated into TiO_2 electrodes.

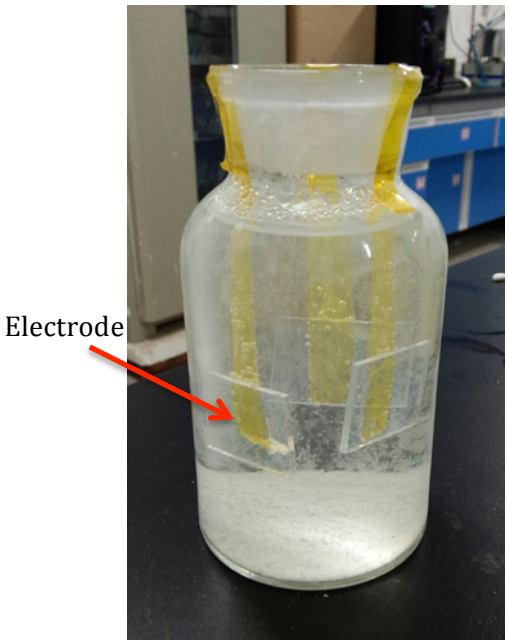

Figure 9: Suspended FTO/ZnO Electrodes

4.1.2 Fabrication of TiO_2 Nanotubes

First, a single solution of 50.0mM ammonium hexafluorotitanate ($[NH_4]_2TiF_6$) and 150.0mM boric acid (H_3BO_3) in 50 mL of DI water was prepared. In order to do so, 0.495g of $[NH_4]_2TiF_6$ was first stirred and dissolved in DI water, and then 0.464g of H_3BO_3 was stirred until everything was dissolved. Three of the FTO/ZnO electrodes were placed in a petri dish, conductive side up, and then submerged in the $[NH_4]_2TiF_6$ and H_3BO_3 solution for 20 minutes. After 20 minutes, the solution was drained and the electrodes, now FTO/TiO_2 electrodes coated with TiO_2 nanotubes, were rinsed thoroughly with DI water. The electrodes were then annealed in a muffle oven; where the temperature was increased from 25°C to 500°C over six hours and maintained at 500°C for four hours. The electrodes were then cooled at room temperature for about six hours. The final electrode looked like Figure 10, below.

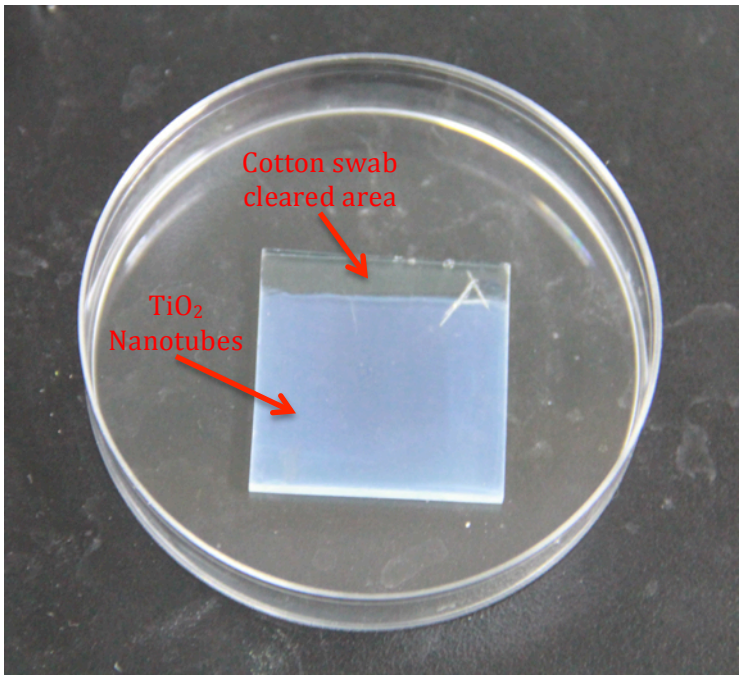

Figure 10: FTO/TiO_2 Nanotubes

4.2 Optimizing the Fabrication Process of a $TiO_2/Bi[VO_4]_3$ Electrode

Bismuth (Bi) was selected as the doping chemical to use on the electrode. bismuth is a group 15 element, meaning the fabricated photoanode would be a n-type semiconductor. A 300mM bismuth(III) vanadate ($Bi[VO_4]_3$) solution was used as the doping chemical on the FTO/TiO_2 electrodes to produce $TiO_2/Bi[VO_4]_3$ electrodes. To optimize the photovoltaic activity of a $TiO_2/Bi[VO_4]_3$ electrode, various independent variables were controlled, such as deposition techniques, cobalt (Co^{2+}) deposition, number of $Bi[VO_4]_3$ deposition layers, and growing time for ZnO nanotubes. To prepare a 300mM $Bi[VO_4]_3$ solution, 300mM bismuth(III) nitrate pentahydrate ($Bi[NO_3]_3{\cdot}5H_2O$) was dissolved in a 2M solution of nitric acid (HNO_3), and then 300mM ammonium metavandate (NH_4VO_3) was dissolved in the same solution. The resulting solution was a yellow, translucent liquid. Figure 11, below shows a not not-to-scale diagram of a FTO/TiO_2 electrode doped with $Bi[VO4]_3$.

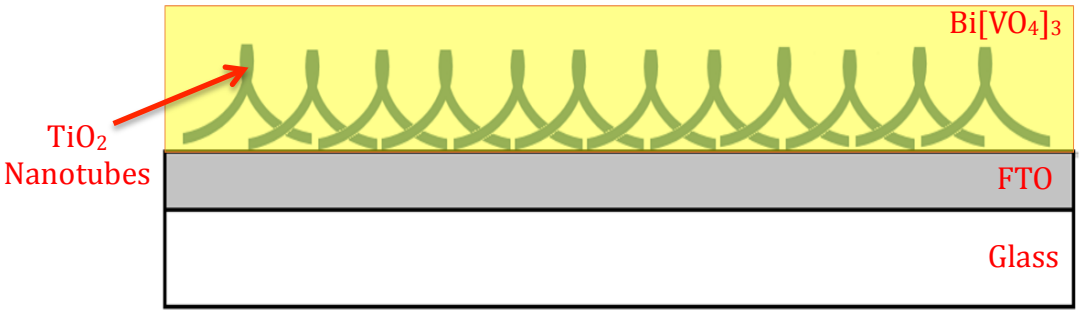

Figure 11: Schematic of a FTO/TiO_2 doped with $Bi[VO_4]_3$

4.2.1 Optimizing the Deposition of $Bi[VO_4]_3$ on to the FTO/TiO_2 Electrode

The spin coating technique was used as the deposition method. In order to optimize the deposition method of $Bi[VO_4]_3$ a large amount of trail and error results were required. There are two independent variables when using the spin coating technique, the RPM and the spin time. In order to determine the optimum

combination, one variable was controlled, while the other variable was kept constant. The spin coating was conducted for 20 seconds, 35 seconds, and 50 seconds; each at 700 RPM, 1500 RPM, and 2000 RPM. For each run, 1 mL of the 300mM $Bi[VO_4]_3$ solution was dropped onto the electrode, with a syringe, at a constant rate over the first 10-15 seconds of the spin cycle. After the spin coating was completed, the electrode was placed on top of a hot plate at 400°C for two hours and then allowed to cool down on a metal plate. First, the optimal deposition method was determined by the visual coating of the $Bi[VO_4]_3$ layer and then by the PEC test if required. After the $Bi[VO_4]_3$ layer had dried, it was fairly easy to determine if the coating was homogeneous or non-homogeneous. Any sample electrode that demonstrated a non-homogeneous coating was discarded. Sample electrodes that had a homogeneous coating of $Bi[VO_4]_3$ were distinguished by the PEC test. The homogeneous sample electrode that recorded the highest photovoltaic activity was considered as the optimal deposition method. The optimized deposition method was then used to fabricate other electrodes for the following optimization variables. Figure 12, below gives an example of a non-homogeneous and a homogeneous electrode.

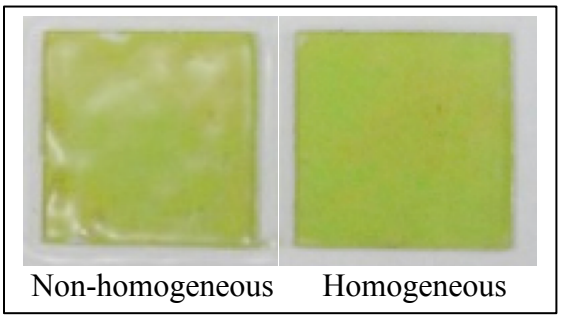

Figure 12: Example of a non-homogeneous and homogeneous electrode

4.2.2 Photo-Deposition of Co^{2+} on the $TiO_2/Bi[VO_4]_3$ Surface

To determine the effect Co^{2+} deposition has on the electrode, a solution comprised of 0.1M KH_2PO_4 and 0.5mM $Co[NO_3]_2$ was dissolved in DI water. This solution was poured into the PEC cell and the $TiO_2/Bi[VO_4]_3$ electrode was suspended into the middle of the cell, making sure none of the alligator clips were submerged in the solution and that the conductive side was facing the lamp. An example of this set up is given in Figure 13. The clear side of the cell was facing the lamp; so all the light could interact with the sample electrode's conducting surface. The interaction between light and applied voltage assists in the deposition of Co^{2+} on to the conducting or $Bi[VO_4]_3$ doped surface. This technique is known as photo-deposition. Once the electrode was submerged, the cathode and the reference electrode were also submerged into the solution. Visible light from the 350W Xeon lamp was exposed on to the working electrode. The electrochemical analyzer then started recording time-current data with the following settings; Voltage (I) = 0.4 V, Time Interval (A) = 0.1 sec, Time (T) = 600 sec, Waiting Time (Q) = 0 sec, Sensitivity (S) = 1×10^{-4} A. The time-current data, however was not an important statistic and was mainly used to assure if the electrode was working as it should be. Cobalt was allowed to deposit itself onto the surface of the $TiO_2/Bi[VO_4]_3$ electrode for 10 minutes. The PEC test was performed to determine the effect of Co^{2+} deposition on the photoanode.

4.2.3 Determining the Optimum Layers of $Bi[VO_4]_3$ Coating

To determine the optimum number of layers of $Bi[VO_4]_3$ coating required to achieve maximum photovoltaic efficiency, various samples of FTO/TiO_2 electrodes

were fabricated. Five different FTO/TiO_2 electrodes were coated with 1, 2, 4, 6, 8, and 10 layers of 300mM $Bi[VO_4]_3$ solution using the optimum deposition method achieved in 4.2.1. Each subsequent layer was coated after the electrode had cooled down to room temperature on the metal plate. The PEC test was conducted on each of the samples to determine the optimum number of layers required.

4.2.4 Determining the Optimum Growing Time for ZnO Nanotubes

Referring back to methodology 4.1.1, we can set the growing time of the ZnO nanotubes as a controlled variable. From theory, the nanotubes grow longer as the reaction time increases. To determine the effect the length of nanotubes have on the photovoltaic efficiency. The FTO/TiO_2 electrode samples were fabricated with reaction times of 3, 6, and 10 hours and then doped with 1 layer of $Bi[VO_4]_3$ coating. A PEC test was performed on the electrodes to compare their photovoltaic activity.

4.3 Characterization of Electrode Samples

Appropriate electrodes were chosen for characterization by PEC tests, SEM, and XRD. Electrodes that showed a homogeneous thin film coating of $[BiVO_4]_3$, to the naked eye, were selected for the PEC test. SEM and XRD tests were only performed on electrodes that provided high photovoltaic activity in the PEC test and on reference electrodes for comparisons.

4.3.1 Photo-electrochemical (PEC) Test

To test an electrode's photovoltaic activity, the PEC test was carried out. Before running the PEC test, the apparatus had to be set up in order to record accurate readings that can be compared existing results. A lab-scale cell, about

2”× 1”× 2”, was used as the habitat for the PEC test. The cell was made from glass, which allows light from a 350W Xeon lamp, to reach the work electrode in the cell. The lamp was equipped with a filter that allows only visible light, wavelengths above 420nm, to pass through. The cathode in the experiment was a platinum strip and the reference electrode was Ag/AgCl. The cell had a $1cm^2$ opening for light to go through, while the rest of the face was covered with an aluminum foil. The electrolyte used in the cell was a 0.1M Na_2SO_4 solution. The work electrode was clipped with an alligator clip with the engraved side of the experimental electrode against the cell wall. This minimized the distance the light had to travel to get to the electrode and therefore minimized the scatter of light due to change in medium. The appropriate wires from the CHI 660C instrument were connected to their respective electrodes. It was made sure the alligator clips are not in contact with the electrolyte solution in the cell. Figure 14, below, shows the set up of the PEC test.

With the help of the CHI electrochemical analyzer and the software CHI 660C, a time-current curve was generated for each work electrode sample. The settings in the program were set accordingly; Voltage (I) = 0 V, Time Interval (A) = 0.1 sec, Time (T) = 400 sec, Waiting Time (Q) = 0 sec, Sensitivity (S) = 1×10^{-4} A. To obtain a voltage-current curve the settings in the program were set accordingly; Voltage (1) = 0 V, Voltage (2) = 1.6 V, Time Interval (A) = 0.1 sec, Waiting Time (Q) = 0 sec, Sensitivity (S) = 1×10^{-4} A. During the ‘dark’ run and the ‘light’ run, it was made sure that all the lights were turned off and the windows were covered. Although during the ‘light’ run, the 350W Xeon lamp was switched on and directed towards the cell. The data was recorded and exported to Microsoft Excel for analysis. The graph uses

conventional current as the y-axis, and therefore the values are negative. However, it is important to understand that the electrons are still flowing from the anode to the cathode.

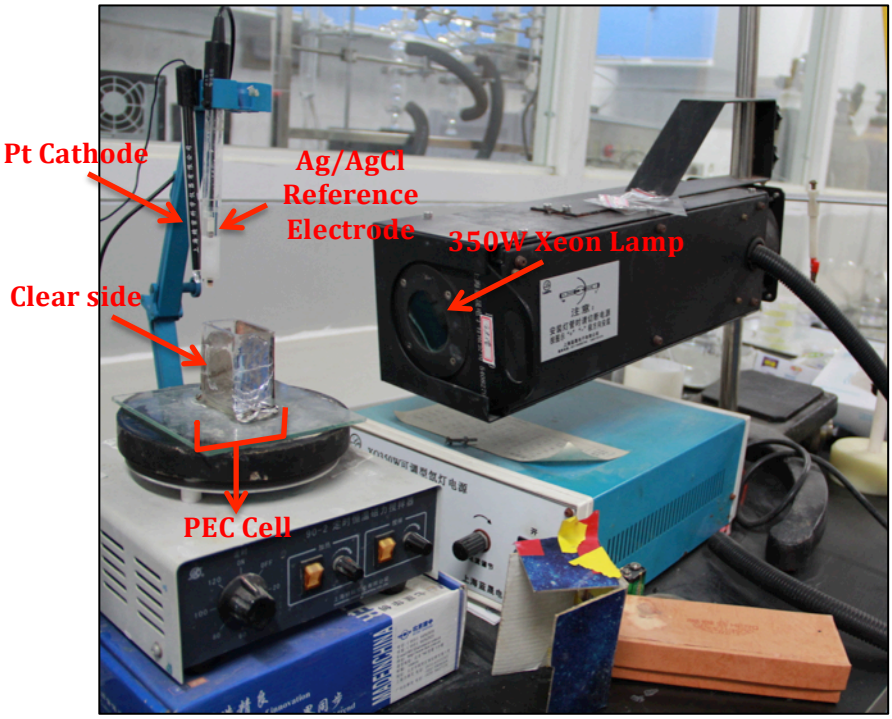

Figure 13: Set-up for PEC Test - 1

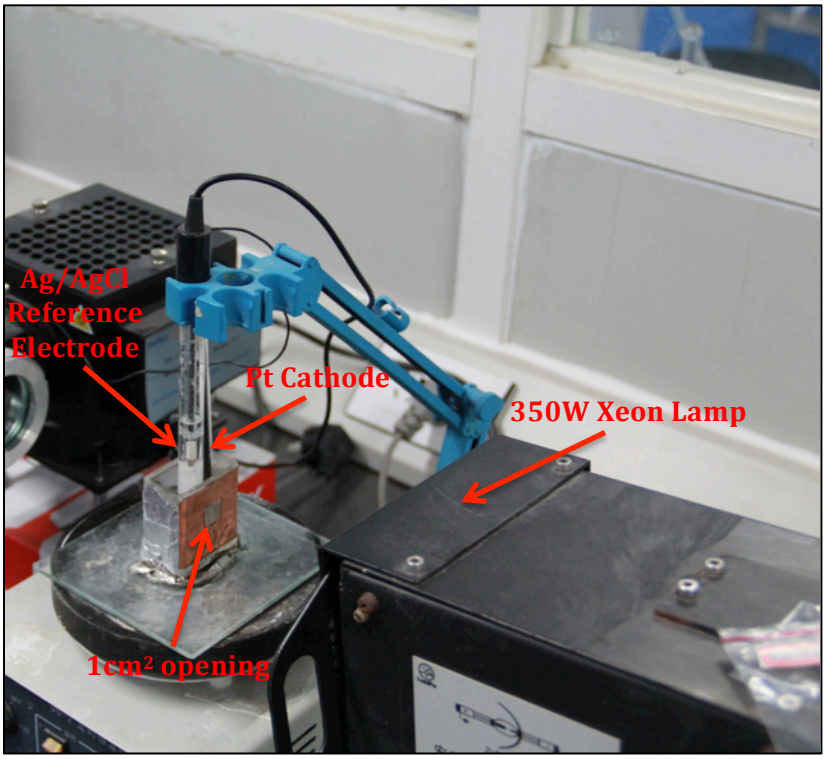

Figure 14: Set-up for PEC Test - 2

4.3.2 XRD and SEM Tests

The XRD test was conducted on the FTO/TiO_2 electrode doped with 1 layer of $Bi[VO_4]_3$ in order confirm its surface chemical composition. This test was necessary, as it would give us the details of the chemicals on the surface of the electrode, leading to a better understanding of the electrode's chemical make-up and whether or not the bismuth molecules were attaching itself to the electrode.

SEM tests were carried out on electrodes that responded well in the PEC test and showed high photovoltaic activity. The SEM images of the selected electrodes were compared to each other for analysis. The test was also run on an FTO/TiO_2 electrode with no doping to determine if the nanoparticles were able to transform to nanotubes successfully.

The SJTU lab technicians carried out the XRD and SEM tests, as the program language was set to Mandarin. Once I received the data and images, I was able to compare and analyze each image to their respective PEC tests.

5 Results & Discussion

Each successfully fabricated FTO/TiO_2 electrode was experimented with, through methods mentioned in 4.2, and run through a PEC test to determine its photovoltaic activity. In this section, only selected electrodes were compared to display the best results. The PEC test for each electrode sample can be found in Appendix B. All of the PEC analysis was performed between the voltage of 0V and 1.2V, as those are the auto reduction and auto oxidation voltages for water, respectively. Data curves in the PEC tests were labeled as per their variables to differentiate them form their counterparts. For example in 5.3 Figure 18, "BiVO4-6 layers" means that the data curve is for an FTO/TiO_2 electrode doped with 6 layers of $Bi[VO_4]_3$ and deposited with cobalt. The sample name does not mention the deposition of cobalt as every sample in comparison was doped with cobalt, and it would not assist in differentiating the samples from one another. Another example of a nomenclature would be "1500 RPM – 50 sec", from section 5.1 Figure 15, which specifies the spin coating method, but does not specify that the electrode is doped with $Bi[VO_4]_3$ as all the sample electrodes in are doped with $Bi[VO_4]_3$.

The experimental results are discussed in the order the methodology was performed in section 4.2. The analysis of the results are discussed thoroughly and compared to values form other works, if available.

5.1 Optimized $Bi[VO_4]_3$ Deposition Method

The deposition method for $Bi[VO_4]_3$ was optimized by varying many process variables as mentioned in 4.2.1. Following is a table summarizing the visual results for each deposition method.

Table 2: Deposition methods that fabricated homogeneous and non-homogeneous electrodes

Spin Coating Speed (RPM)	Spin Coating Time (sec.)	Visual Description of $Bi[VO_4]_3$ Coating
700	20	Very non-homogeneous
	35	Non-homogeneous
	50	Non-homogeneous
1500	20	Non-homogeneous
	35	Slightly non-homogeneous
	50	Homogeneous
2000	20	Slightly non-homogeneous
	35	Homogeneous
	50	Homogeneous

As seen in Table 2, three electrodes showed a homogeneous coating of $Bi[VO_4]_3$, while the rest showed a non-homogeneous coating and were therefore discarded. A relationship between spin coating speed and time is noticeable as the greater the RPM and longer the spin coating is carried out, the more homogeneous the coating on the electrode. This is due to the fact that the bismuth solution is composed of powdery particles, which require high-speed and long spin times to spread across the entirety of the electrode. However, it was important to deposit only one layer of the $Bi[VO_4]_3$ solution as there is no direct measurable relationship between the spin coating technique and the number of layers. Therefore the number of layers would be a controlled variable. The three homogeneous samples were then analyzed through the PEC test. The graph of their photovoltaic activity is represented in Figure 15, below.

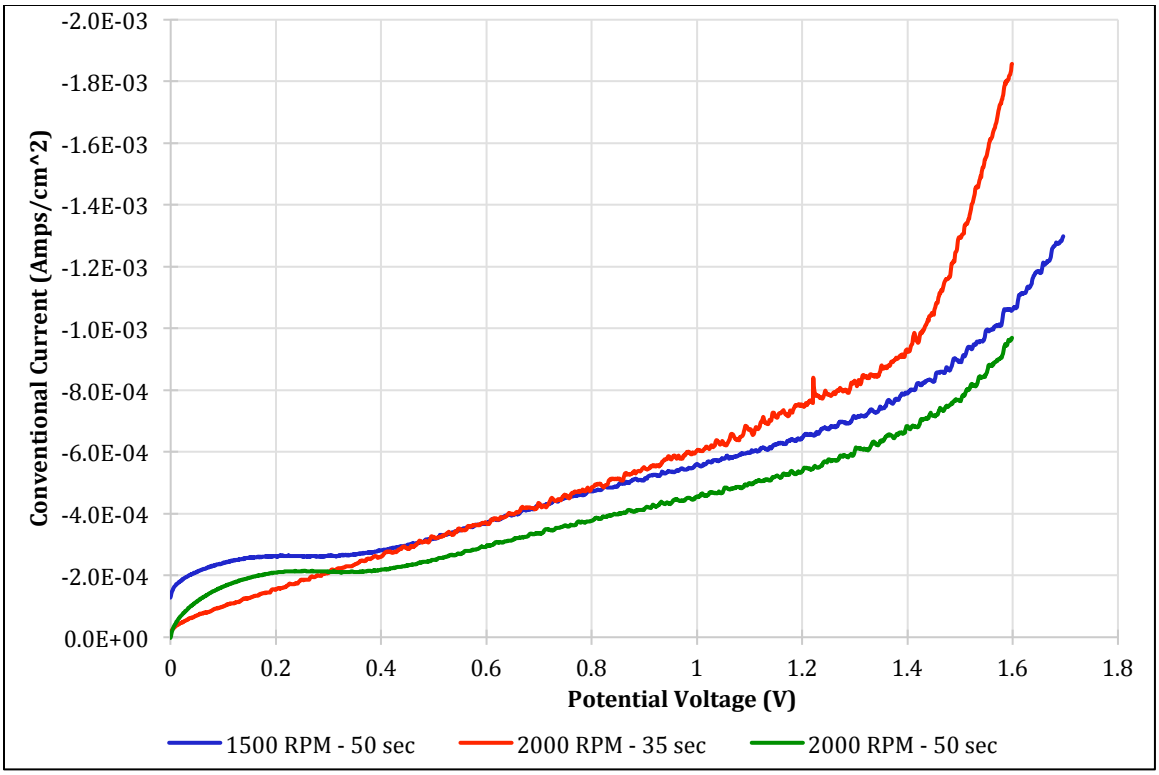

Figure 15: PEC test of 300 mM $Bi[VO_4]_3$ homogeneous electrodes at different coating processes

As observed in Figure 15, the electrode that provided the highest current at a voltage of 1.2 was deposited with 1mL of 300mM of $Bi[VO_4]_3$ solution at a speed of 2000 RPM for 35 seconds. However, the graph shows that between the voltage of 0V and 0.4V the electrode deposited at 2000 RPM for 50 seconds performs slightly better than the one deposited at 2000 RPM for 35 seconds. Also, the electrode deposited at 2000 RPM for 35 seconds only betters the electrode deposited at 1500 RPM for 50 seconds after a voltage of 0.8V. However, considering 1.2V as our maximum operating voltage the electrode deposited at 2000 RPM for 35 seconds was considered the optimized one. The optimized sample electrode was then compared with the PEC test run of an FTO/TiO_2 electrode with no chemical doping, fabricated through methodology in 4.1. Figure 16, below, shows the effect of doping an FTO/TiO_2 with $Bi[VO_4]_3$.

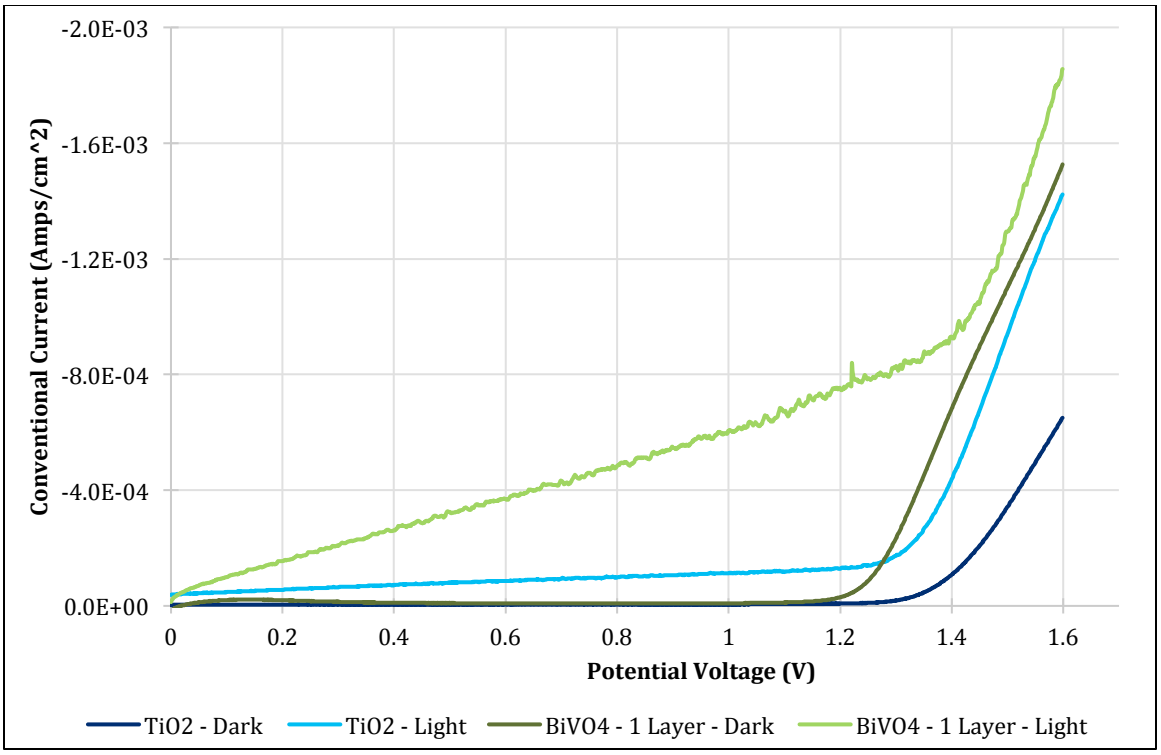

Figure 16: PEC test for FTO/TiO_2 with and without $Bi[VO_4]_3$ coating

Figure 16 shows a clear increase in conventional current after the FTO/TiO_2 electrode was doped the with $Bi[VO_4]_3$. The figure shows a 'dark' run, with no lights on, and a 'light' run, with the lamp directed at the PEC cell. It was necessary to determine the photovoltaic activity in the dark to assure there is no current output as there is no light for catalysis. As observed in the 'dark' runs, photovoltaic activity rises after about 1.2V as redox reactions are initiated without the assistance of light as catalyst. At a voltage of 1.2V, the conventional current density increased from -1.29×10^{-4} Amps/cm^2 to -7.52×10^{-4} Amps/cm^2, which is an increase by 483%. The deposition of $Bi[VO_4]_3$ has a large, positive effect on the efficiency of the photoanode.

The values received from this experimental data can be put into context from work conducted by Thillai Natarajan et al. on photocatalytic degradation of Rhodamine B dye via bismuth-doped TiO_2 nanotubes (Bi-TNT), bismuth-doped TiO_2

nanoparticles (Bi-TNP), TiO_2 nanotubes (TNT), and TiO_2 nanoparticles (TNP). They were able to show that the TNT had 68% more surfaces area allowing for great light absorbance. From the four semiconductors, their studies revealed that Bi-TNT was 4.16 times, increase by 316%, higher at photocatalytic degradation (Natarajan, Baja, Tayade, et al., 2013). This result is similar to the result received though this experiment, which was an increase in current density by 483% or 5.38 times. Differences in values are expected as Natranjan et al. measured photocatalytic degradation where as this experiment, measured current density. However, the effect of bismuth doping is similar in both cases. Liu et al. (2011) were able to achieve a current density of about 2.5×10^{-4} Amps/cm^2 with their FTO/TiO_2 electrode using UV light as their catalyst. This experiment was conducted with visible light and therefore the energy supplied was lower when compared to UV illumination.

5.2 Effect of Cobalt Deposition

After the deposition of cobalt, Co^{2+}, on to the $Bi[VO_4]_3$ doped electrode surface, the photovoltaic activity of the sample electrodes were tested using the methodology in 4.2.2. Figure 17, below, shows the effect of depositing cobalt on to the $Bi[VO_4]_3$ surface.

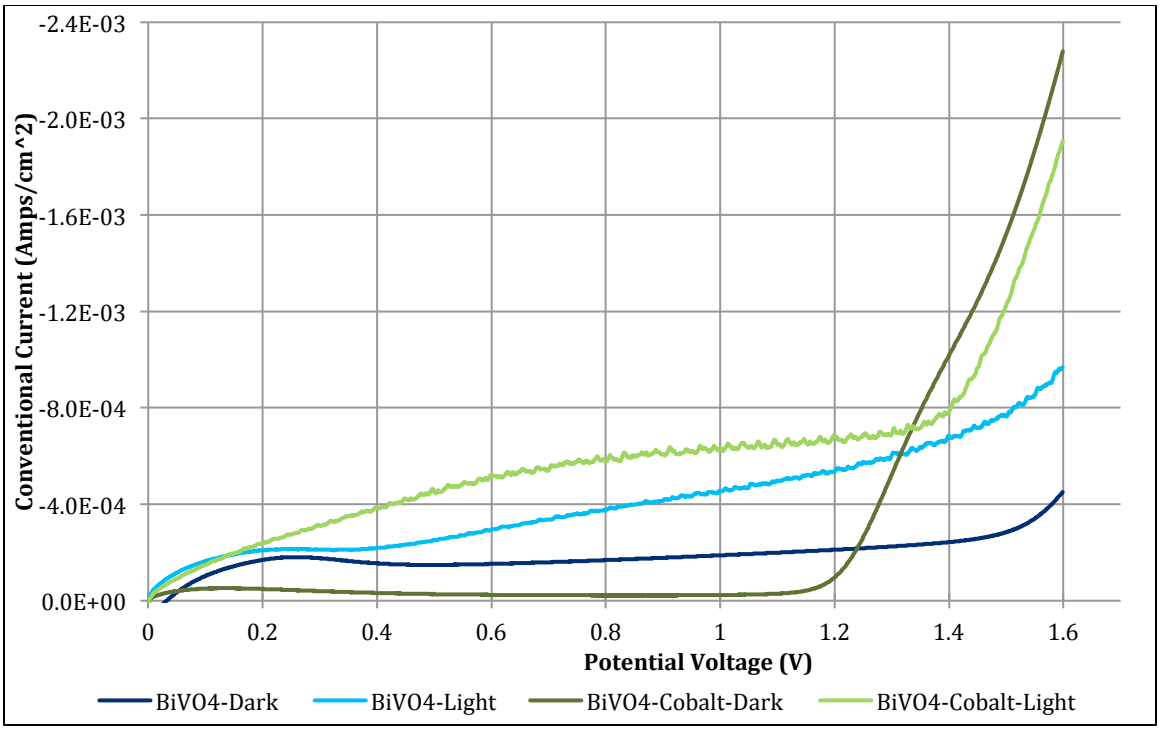

Figure 17: PEC test of $TiO_2/Bi[VO_4]_3$ electrode with and without Cobalt coating

It is evident from Figure 17 that the cobalt deposition increased the photovoltaic activity of the electrode, as seen by the higher current output from the 'BiVO4-Cobalt-Light' run when compared to the 'BiVO4-Light' run. However, it is important to note that the 'BiVO4-Dark' run had some photovoltaic activity, which would be considered abnormal, as there was no light for photocatalysis.

Despite minor flaws in the data, the experimental value holds true to results attained by different experiments. Lin Li and LiCheng Sun, were able to prove the effectiveness of photo-depositing cobalt on to a n-type TiO_2 semiconductor. They used a higher watt Xeon lamp and a longer photo-deposition time of 1 hour, to achieve a current density output of 5.0×10^{-3} Amps/cm^2 (Lin & LiCheng, 2012). Their results were higher as they had a stronger light source, and had optimized the thickness of the TiO_2 film. Cobalt proved to play and important role in improving the

photovoltaic activity as the hydroxides of cobalt have strong electrochemical, catalytic, and optical properties. Hydroxides of cobalt are being used in technologies such as supercapacitors, electrocatalysts, and electrochemical electrodes. Therefore, it has been proven to improve photovoltaic activity, as shown in results through this experiment.

5.3 Optimum Layers of $Bi[VO_4]_3$ Coating

Using the optimum deposition method and the cobalt deposition, the optimum number of layers of $Bi[VO_4]_3$ coating was determined using methodology mentioned in 4.2.3. Figure 18, below, summarizes the PEC data received from 1, 2, 4, 6, 8, and 10 layers of $Bi[VO_4]_3$ coating.

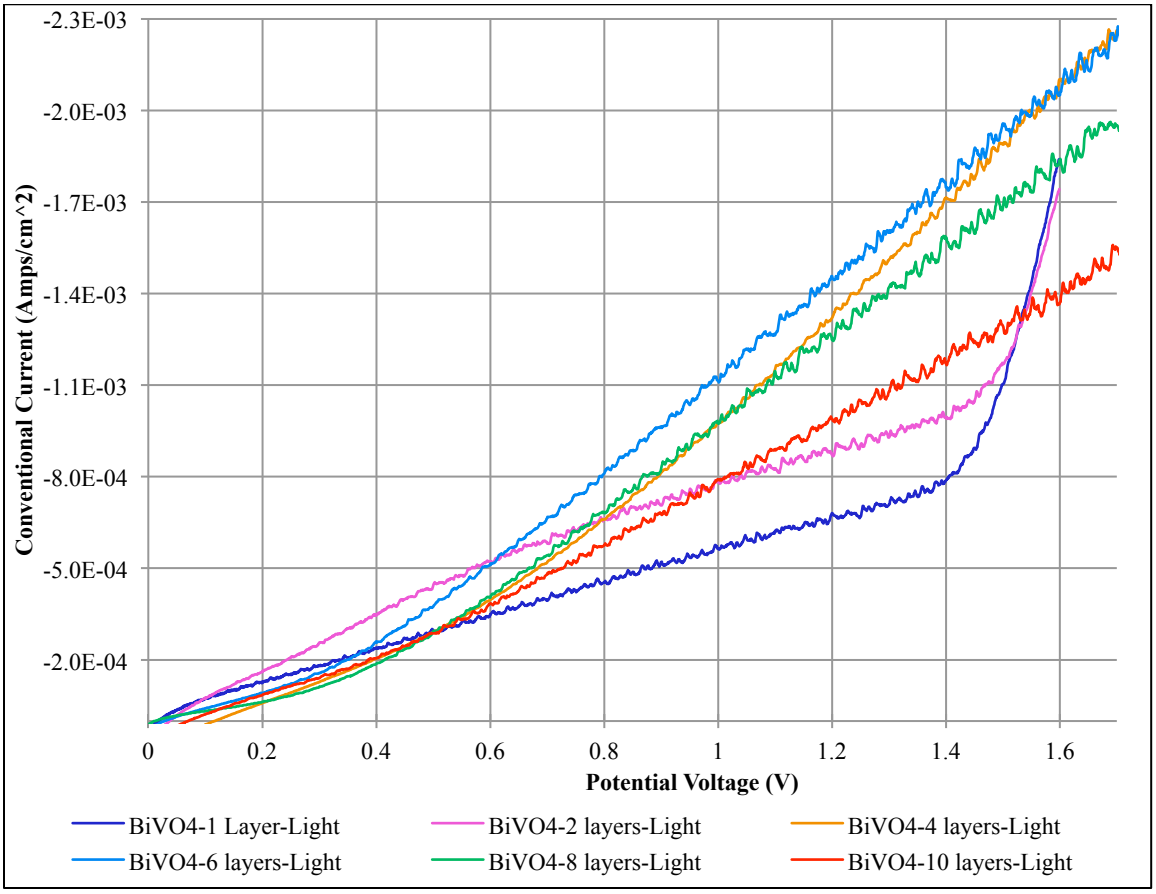

Figure 18: PEC test for $TiO_2/Bi[VO_4]_3$ electrodes with different number of layers

It is observed from Figure 18 that a coating of 6 layers of $Bi[VO_4]_3$ produces the highest amount of current at a voltage of 1.2V. A clear trend is visible, where the conventional current increases as the number of $Bi[VO_4]_3$ layers increase, till the current reaches a maximum with the 'BiVO4-6 layers-Light' run, and then the conventional current decreases again. Therefore, it can be concluded that the optimized number of $Bi[VO_4]_3$ layers is 6. Considering a single layer of $Bi[VO_4]_3$ coating on the FTO/TiO2 electrode as the base point and 6 layers of $Bi[VO_4]_3$ coating as the optimum point, the percent increase in current density at a voltage of 1.2V can be calculated to 114% or an increase in current density by a factor of 2.14. The addition of extra layers of bismuth resulted in an increase in current density, as it was able to absorb a greater range and amount of light. However, the photovoltaic benefit from increasing the number of $Bi[VO_4]_3$ layers diminishes after 6 layers. A reason as to why this occurs could be attributed to amount of bismuth particles present on the surface, such that it creates negative effects. Further analysis in section 5.6, through SEM tests, explains these negative impacts on the photovoltaic activity of electrodes with excess layers of bismuth through surface morphology.

5.4 Optimum Growing Time for ZnO Nanotubes

The growing time of ZnO nanotubes was varied between 3, 6, and 10 hours to determine the optimum reaction time to achieve maximum current output, as per methodology in 4.2.4. The PEC curves for each reaction time are displayed in Figure 19, below.

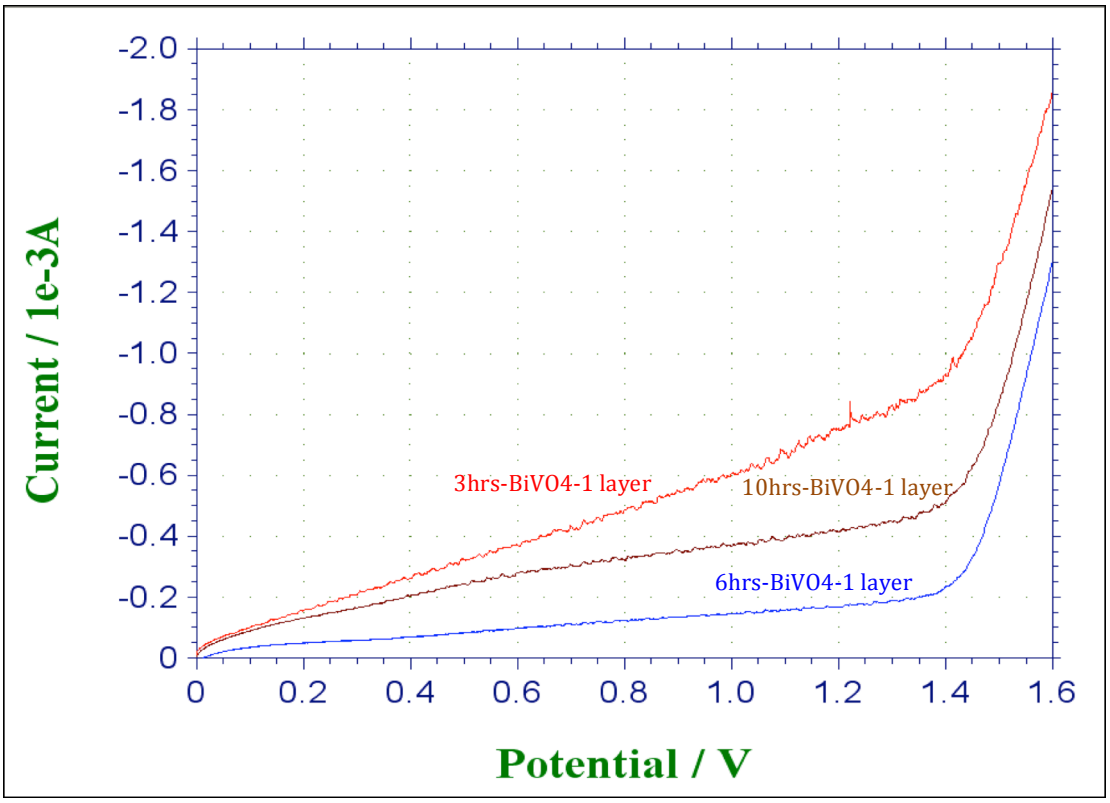

Figure 19: PEC Test for different ZnO nanotubes growing time

It is evident from Figure 19 that the electrode with the ZnO nanotube growing time of 3 hours displayed the highest current output. However, a clear trend is not observable as the when the reaction time is increased to 6 hours, the current output drops and when the reaction time is further increased to 10 hours, the current output increase, but doesn't surpass the electrode with a reaction time of 3 hours. Along with the quantitavie data, qualitative data was recorded for the 3 electrode samples. The TiO_2 nanotubes seemed to get more brittle as the reaction time was extended. Due to the increased length, the tubes were easily blown off or scratched off the surface of the tube as it bears less force on the glass itself. Therefore, from available data, it was fair to conclude that a reaction time of 3 hours

for the ZnO nanotubes to grow is the optimal reaction time to achieve efficient photovolatic activity.

5.5 X-ray Diffraction

The XRD test was carried out on the FTO/TiO_2 electrode optimized form section 5.1. This sample electrode was an FTO/TiO_2 electrode deposited with a 300mM $Bi[VO_4]_3$ solution via spin coating at 2000 RPM for 35 seconds. The primary objective of this test was to verify the chemical composition of the electrode's surface and to verify the deposition on bismuth on the surface. Figure 20 shows the X-ray spectroscopy received for this electrode sample.

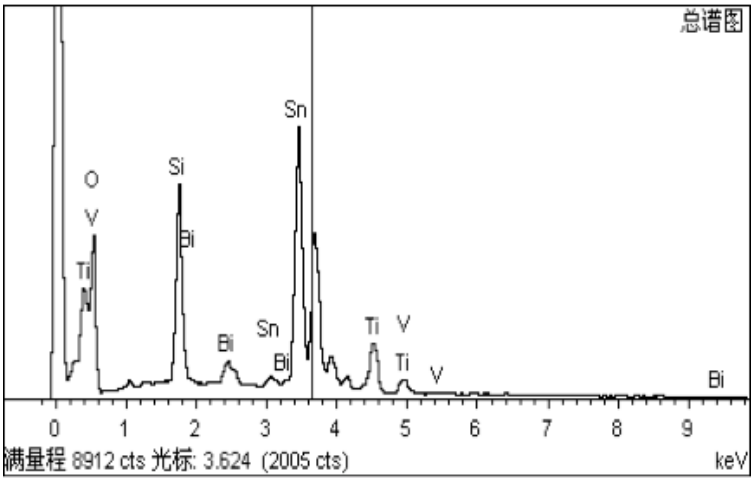

Figure 20: X-ray spectroscopy for sample electrode

Figure 20 indicates all the elements that were detected through by the XRD test. The elements from the graph are represented in terms of weight percent and atomic percent in Table 3, below.

Table 3: Weight % and atomic % of different elements on the FTO/TiO_2 Coated with 1 Layer of $Bi[VO_4]_3$ sample electrode achieved from method 4.2.1

Element	Weight %	Atomic %
O	45.32	79.74
Si	7.61	7.63
Ti	4.40	2.59
V	0.76	0.42
Sn	38.83	9.21
Bi	3.08	0.42
Total	100.00	100.00

As seen in Figure 20 and Table 3, bismuth is present on the surface as 3.08 weight % of all the elements. According to the data in the table, titanium exists as 4.40 weight % of all the elements on the surface, whereas no zinc is present. This indicates that all of the ZnO nanotubes were successfully converted to TiO_2 nanotubes, signifying a successful reaction and fabrication process.

5.6 Scanning Electron Microscopy

The SEM test was carried out for two different purposes. First, was to verify the surface structure of the FTO/TiO_2 electrode without any doping. The ZnO nanoparticles were transformed to nanotubes and then reacted using the methodology in 4.1.2 to TiO_2 nanotubes. The SEM of the FTO/TiO_2 electrode was generated to verify the tubular structure of TiO_2 on the surface of the electrode. The second purpose of the SEM test was to understand the effect the number of $Bi[VO_4]_3$ layers had on the surface morphology. The electrodes selected for this test were the electrodes coated with 1, 6, and 10 layers of $Bi[VO_4]_3$. Below are the SEM images for all three of the electrodes.

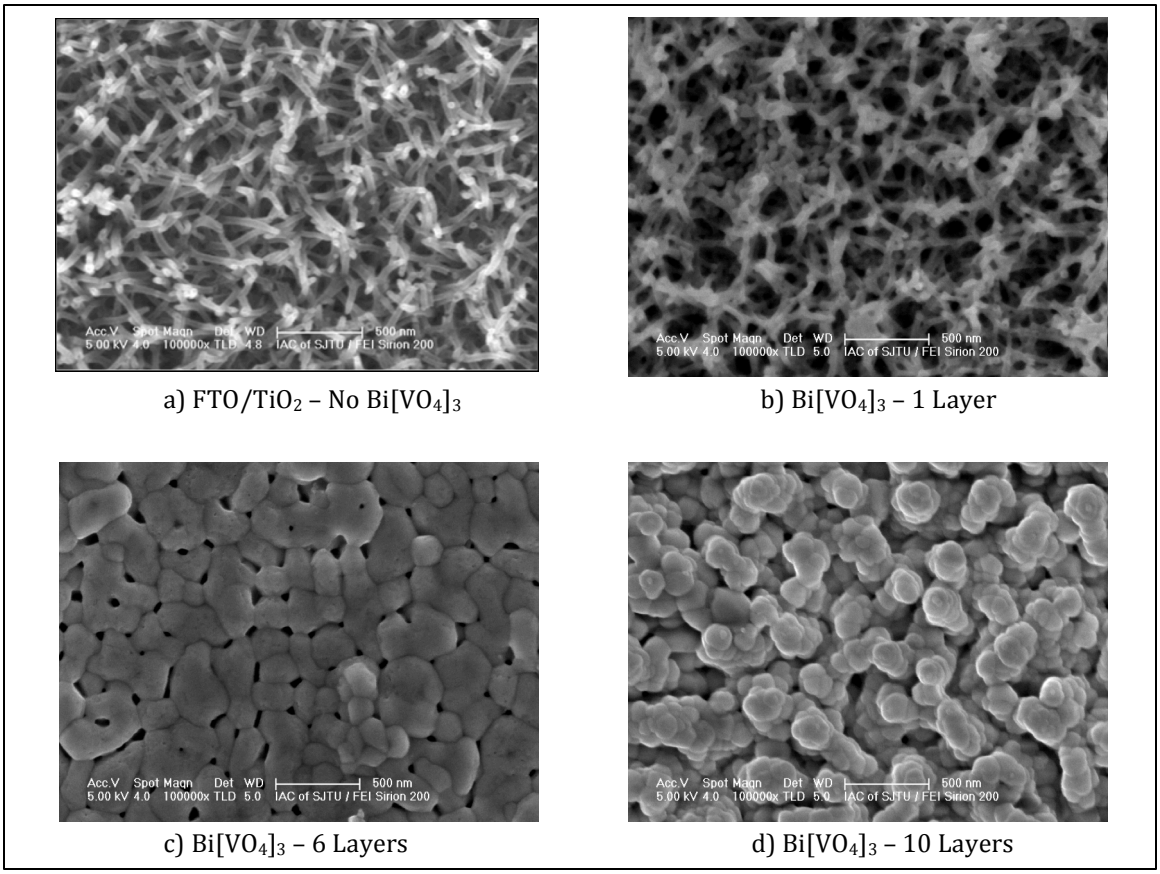

a) FTO/TiO_2 – No $Bi[VO_4]_3$ b) $Bi[VO_4]_3$ – 1 Layer

c) $Bi[VO_4]_3$ – 6 Layers d) $Bi[VO_4]_3$ – 10 Layers

Figure 21: SEM images comparing different layers of $Bi[VO_4]_3$

The SEM image of the un-doped FTO/TiO_2 electrode surface confirms the presence of nano-tubular TiO_2. However, the nanotubes are not upright, but are entangled amongst other nanotubes.

There is a clear effect of bismuth doping on the TiO_2 nanotubes and the surface morphology. After the first layer of $Bi[VO_4]_3$ is coated, several TiO_2 nanotubes attach themselves to a spot of $Bi[VO_4]_3$. This is noticed in several areas and this also creates holes in the electrodes, represented as black in Figure 21 b). The TiO_2 nanotubes are no longer visible once 6 and 10 layers of $Bi[VO_4]_3$ have been doped onto the surface. Between 21 b) and 21 c) the spots of bismuth became larger and more dense. Most of the empty space from Figure 21 b) is no longer visible as the bismuth covers the entire surface. The bismuth forms a layer on top of the TiO_2

nanotubes. Whereas, when comparing Figure 21 c) and d), we see a lot more spots of bismuth. With c) the bismuth formed a layer over the surface of the electrode whereas, in d) it seems as if the bismuth has coated the TiO_2 nanotubes. The electrode used in Figure d) also seemed very close to being opaque, and maybe the lack of light interacting with the conducting surface resulted in a lower photovoltaic activity. Another possible explanation for the decrease in photovoltaic activity as bismuth layers were increased past 6 layers could be attributed to the negative impact of excess bismuth particles. Bismuth particles could have overcrowded the electrode surface such that not all the particles were bound to TiO_2 nanotubes. These bismuth particles would absorb the light, but would not be able to excite the electrons in the TiO_2's valence band, as they were not able to form a heterojunction with TiO_2 nanotubes. The addition of bismuth past a specific amount created free, unattached bismuth, which was creating inefficiencies. In this experiment, that point was beyond 6 layers of 300 mM $Bi[VO_4]_3$.

6 Conclusions

The two main objectives of this project were to optimize the fabrication process of a bismuth-doped FTO/TiO_2 electrode to improve the photoanode's efficiency and to characterize the photoanode through XRD and SEM tests. After analyzing the results, certain conclusions can be drawn to fulfill the primary objectives. First, the optimized fabrication process comprises of, growing the ZnO nanotubes for 3 hours on FTO electrodes and then converting them to TiO_2 nanotubes. Then doping the FTO/TiO_2 electrodes with 6 layers of $Bi[VO_4]_3$ coating, accomplished via spin coating technique at 2000 RPM for 35 seconds. Finally, cobalt was deposited onto the doped-surface via the photo-deposition method for 10 minutes. Figure 22, below, summarizes the optimized fabrication process.

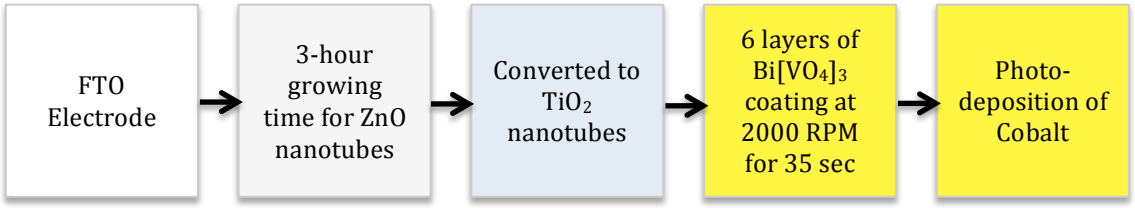

Figure 22: Optimized fabrication process

A photoanode fabricated using this process, yielded the maximum current density output under visible light, which was -1.46 mA/cm^2. Our base electrode was the FTO/TiO_2 electrode, which yielded a current density output of -0.129 mA/cm^2. The optimized electrode was able to yield 11.3 times more current than the base FTO/TiO_2 electrode. Within the process optimization, photovoltaic efficiency was greatly increased by the optimized deposition method and number of layers of $Bi[VO_4]_3$, 483% and 114% respectively. The overall increase in photovoltaic

efficiency was recorded as 1030%, considering the FTO/TiO_2 electrode as the base point.

Furthermore, results from the XRD and SEM tests proved to be relevant for verifying the chemical composition of the electrode and in understanding the effect of bismuth deposition on the surface texture. The XRD test confirmed the deposition of bismuth on the surface of the electrode. The SEM images of the FTO/TiO_2, and the 1, 6, and 10 layers of $Bi[VO_4]_3$ electrode samples showed that adding additional layers of $Bi[VO_4]_3$ resulted in thicker, non porous spots forming above the TiO_2 nanotubes. The 6-layer coating provided the adequate amount of doping chemical without hampering the photovoltaic activity.

In conclusion, bismuth proved to be an effective doping chemical on an FTO electrode coated with TiO_2 nanotubes. The optimized fabrication process further improved the efficiency of the electrode, yielding a greater current density. XRD and SEM tests verified the chemical composition of the electrode surface and the effect of bismuth doping on the TiO_2 nanotubes.

7 Recommendations & Future Work

Though the results were positive and hopeful, the number of trials for conducted to determine the optimization results were not enough to determine its repeatability. Due to the time constraint and a time consuming process for fabricating the electrodes, not more than 2 trials were conducted for each independent variable. This experiment was conducted over a period of 8 weeks, in which the fabrication process first had to be learned and then the independent variables could've been altered. Each batch of FTO/TiO_2 electrodes took about 2 days to fabricate and an additional 1-2 days to fabricate the bismuth-doped FTO/TiO_2 electrodes, depending on the independent variable. It would be recommended that this work be repeated again with as many as 3 to 5 trials for each process variable to verify the precision of the results. This would potentially remove any errors from the experiment. An error in this report due to the lack of trials included the inconsistent trend of ZnO growing time. It would also be recommended that if a sample electrode showed any photovoltaic activity during its 'dark' PEC run, it should not be considered as part of the results and a new, more representative electrode should be tested. Even though, enough independent process variables were tested in this lab to determine an approximate optimum variable, more independent variables should be test. For example, to optimize the layers of $Bi[VO_4]_3$, electrode sample with 5 and 7 layers should also be tested to confirm the optimum number of layers.

Bismuth proved to be a successful doping chemical as it allowed visible light to act as a catalyst thus improving the photoanode's efficiency. Due to these

promising results, further tests should be carried out using bismuth to further optimize the fabrication process resulting in a higher current density yield. A study by Xiaofang et al. (2012) showed that the addition of triethanolamine (TEA) to bismuth-doped TiO_2 electrodes improved the performance of the photoanode. Their results showed that the addition of TEA changed the surface morphology by reducing the particle size of the bismuth coating and making the surface seem more porous. The TEA addition also improved the light absorption performance of the anode due to a more porous surface and a reduction in the band gap, indicated by the red shift of visible light (Xiaofang, Hongwu, & Yanqin, 2012). Adding TEA to our optimized electrode sample could result in a more efficient photoanode. Since TEA reduces the particle size and makes it more porous, layers of $Bi[VO_4]_3$ greater than 6 can should be tested again to see the effect it would have on the SEM images and the photovoltaic activity. Furthermore, Tao Pian, et al. (2011) showed that creating a more porous TiO_2 nanotube layer results in a greater absorption of visible light. This increases the photovoltaic activity, as more light is available for photocatalysis (Pian, Lin, Chen, et al., 2011). Future work can be targeted towards creating and characterizing a more porous TiO_2 surface.

References

Adeli, B. (Designer). (2013, March 26). Band-gapstructureofsomesemiconductorsandtheirlimitationsforwatersplitting. [Web Photo]. Retrieved from http://jss.ecsdl.org/content/2/7/Q118/F2.large.jpg

conduction band. (n.d.) The American Heritage® Science Dictionary. (2005). Retrieved February 11 2014 from http://www.thefreedictionary.com/conduction+band

Doman, L. E. U.S. Department of Energy, Office of Energy. (2013). *International energy outlook 2013* (DOE/EIA-0484). Retrieved from U.S. Energy Information Administration website: http://www.eia.gov/forecasts/ieo/pdf/0484(2013).pdf

Du, Z., Li, H., & Gu, T. (2007). A state of the art review on microbial fuel cells: A promising technology for wastewater treatment and bioenergy. *Biotechnology Advances*, *25*(5), 464-482. Retrieved from http://www.sciencedirect.com/science/article/pii/S0734975007000547

Hashimoto, K., Irie, H., & Fujishima, A. (2005). Tio2 photocatalysis: A historical overview and future prospects. *Japanese Journal pf Applied Physics*, *44*(12), 8269-8285. doi: 10.1143/JJAP.44.8269

Hoffman, M. R., Martin, S. T., Choi, W., et.al., (1995). Environmental applications of semiconductor photocatalysis. (95), 69-96. doi: 10.1021/cr00033a004

Kumar, P. (2013). Semiconductor basics. 2-7. Retrieved from http://www.slideshare.net/PankajKumar40/semiconductor-basics

Lin, L. & LiCheng, S. (2012). Electrochemical water oxidation by photo-deposited cobalt-based catalyst on a nano-structured TiO2 electrode. *Science China Chemistry*, *55*(9). doi: 10.1007/s11426-012-4551-8

Liu, Y., Li, J., & Zhou, B. (2011). A tio2-nanotube-array-based photocatalytic fuel cell using refractory organic compounds as substrates for electricity generation. *Chemical Communications*, *44*(37), 8269-8285. doi: 10.1039/C1CC13388H

Liu, Y., Li, J., Zhou, B., et.al., (2011). Efficient electricity production and simultaneously wastewater treatment via a high-performance photocatalytic fuel cell. *Water Research*, *45*(13), 3991-3998. Retrieved from http://www.sciencedirect.com/science/article/pii/S0043135411002673

Liu, Y., Li, J., Zhou, B., et.al., (2011). Photoelectrocatalytic degradation of refractory organic compounds enhanced by a photocatalytic fuel cell. *Applied Catalysis B: Environmental*, *111-112*(12), 485-491. Retrieved from http://www.sciencedirect.com/science/article/pii/S092633731100508X

Nakamura, T. K. UNEP, Freshwater and Marine Ecosystems Branch. (n.d.). *Wastewater*. Retrieved from UNEP website: http://www.unep.org/ecosystemmanagement/Portals/7/Documents/factsheets/Wastewater FactSheet web.pdf

Natarajan, T. S., Natarajan, K., Bajaj, H. C., & Tayade, R. J. (2013). Enhanced photocatalytic activity of bismuth-doped TiO2 nanotubes under direct sunlight irradiation for

degradation of Rhodamine B dye. *Journal of Nanoparticle Research*, *15*(1669). doi: 10.1007/s11051-013-1669-3

Natural Resources Management and Environment Department, (1992). *Wastewater treatment and use in agriculture* (0254-5284). Retrieved from FAO Corporate Document Repository website: http://www.fao.org/docrep/T0551E/T0551E00.htm

Nave, C. R. (2014). Band theory of solids. Retrieved from http://hyperphysics.phy-astr.gsu.edu/hbase/solids/band.html

Rodrigues da Silva, M., Lucilha, A. C., Afonso, R., et.al., (2013). Photoelectrochemical properties of fto/m-bivo4 electrode in different electrolytes solutions under visible light irradiation. *Ionics*, *20*(1), 105-113. doi: 10.1007/s11581-013-0967-1

Ross, N. Pacific Institute, (2010). *World water quality facts and statistics*. Retrieved from World Water Day website: http://www.pacinst.org/wp-content/uploads/2013/02/water_quality_facts_and_stats2.pdf

Scanning electron microscopy (sem). (2013). Informally published manuscript, Science Education Resource Center, , Available from NSF. Retrieved from http://serc.carleton.edu/research_education/geochemsheets/techniques/SEM.html

Pian, T., Lin, B., Chen, Y., Kuang, J., Zhang, K., & Fu, L., (2011). Pillared Nanocomposite TiO_2/Bi-Doped Hexaniobate with Visible-Light Photocatalytic Activity. *The Journal of Physical Chemistry*. doi: 10.1021/jp1097553

Tripathi, B., Yadav, P., & Kumar, M. (2013). Theoretical upper limit of short-circuit current density of TiO_2 nanorod based dye-sensitized solar cell. *Results in Physics*, *3*. 182-186. http://ac.els-cdn.com/S2211379713000284/1-s2.0-S2211379713000284-main.pdf?_tid=abf55cba-c682-11e3-937d-00000aab0f6c&acdnat=1397775208_b412f91c39cc9f18ea29d30323a50231

Types of fuel cells. (2014). Retrieved from http://www.fuelcells.org/base.cgim?template=types_of_fuel_cells

valence band. (n.d.) McGraw-Hill Dictionary of Scientific & Technical Terms, 6E. (2003). Retrieved February 11 2014 from http://encyclopedia2.thefreedictionary.com/valence+band

Xiaofang, C., Hongwu, F., & Yanqin, W., (2012). Preparation of Bi-doped TiO2 modified by TEA and Its Enhanced Photocatalytic Properties under visible light illumination. *Advances in Intelligent Systems Research*. doi: 10.2991/emeit.2012.102

X-ray diffraction. (n.d.). Retrieved April 11, 2014, from http://www.merriam-webster.com/dictionary/x-ray%20diffraction

Zandaryaa, S. UNESCO, UNESCO Division of Water Sciences. (2011). *Global challenge of wastewater*. Retrieved from SIWI website: http://www.worldwaterweek.org/documents/WWW_PDF/2011/Sunday/K21/The-Malin-Flakenmark-Seminar/Global-challenge-of-wastewater-Example-from-different-continents.pdf

Glossary

Abbreviations

BOD	Biological Oxygen Demand
CBD	Chemical Bath Deposition
DI	Deionized
FTO	Fluro-doped Tin Oxide
MFC	Microbial Fuel Cell
PEC	Photoelectrochemical
PEM	Proton Exchange Membrane
PFC	Photocatalytic Fuel Cell
RPM	Rounds Per Minute
SEM	Scanning Electron Microscopy
SJTU	Shanghai Jiao Tong University
TCF	Transparent Conducting Film
TCO	Transparent Conducting Oxide
UV	Ultraviolet
XRD	X-Ray Diffraction
YSZ	Yttria-stabalized zirconia

Terminology

Anode – is a negatively charged electrode of an electrical device, from which electrons flow out of

Cathode – is a positively charged electrode of an electrical device, where electrons flow into

Conduction Band – is the level of energy that is required to pull an atom's valence electron

Electrolyte – a medium through which selective ions can be transported from on side of a cell to the other

Photocatalysis – a reaction in which, light is absorbed by a chemical and acts as a catalyst to initiate a reaction

Photovoltaic – relating to the production of electric current when a substance is exposed to light

Valence Band – is the highest level of energy in an atom where electrons are present, also known as the valence electrons

Appendices

Appendix A: Sample Calculations

A.1 Determining the Mass Required to Prepare a Molar Solution

Example: 50mL of a 50.0mM solution of $[NH_4]_2TiF_6$

$$M = \frac{n}{V}$$

$$MW_{[NH_4]_2TiF_6} = 197.93\frac{g}{mol}$$

$$50.0mM = 0.05M = \frac{n}{0.05L}$$

$$n = MV = 0.05M * 0.05L$$

$$n = 0.0025\ mols$$

$$m = n * MW = 0.0025\ mols * 197.93\frac{g}{mol}$$

$$\boldsymbol{m = 0.495g}$$

Therefore, 0.495g of $[NH_4]_2TiF_6$ was dissolved in 50mL of DI water to make a 50mM solution.

A.2 Determining Percent Change

Example: Photovoltaic activity from FTO/TiO_2 electrode to FTO/TiO_2 doped with 1 layer of $Bi[VO_4]_3$

$$\%\ Change = \left(\frac{|New\ Value - Old\ Value|}{Old\ Value}\right)\times 100$$

$$\%\ Change = \left(\frac{|-7.52\times10^{-4} + 1.29\times10^{-4}|}{-1.29\times10^{-4}}\right)\times 100$$

$$\boldsymbol{\%\ Change = 483\%}$$

Appendix B: Voltage-Current Graph for Each Electrode Sample

B.1 PEC Tests for FTO/TiO_2 Electrodes

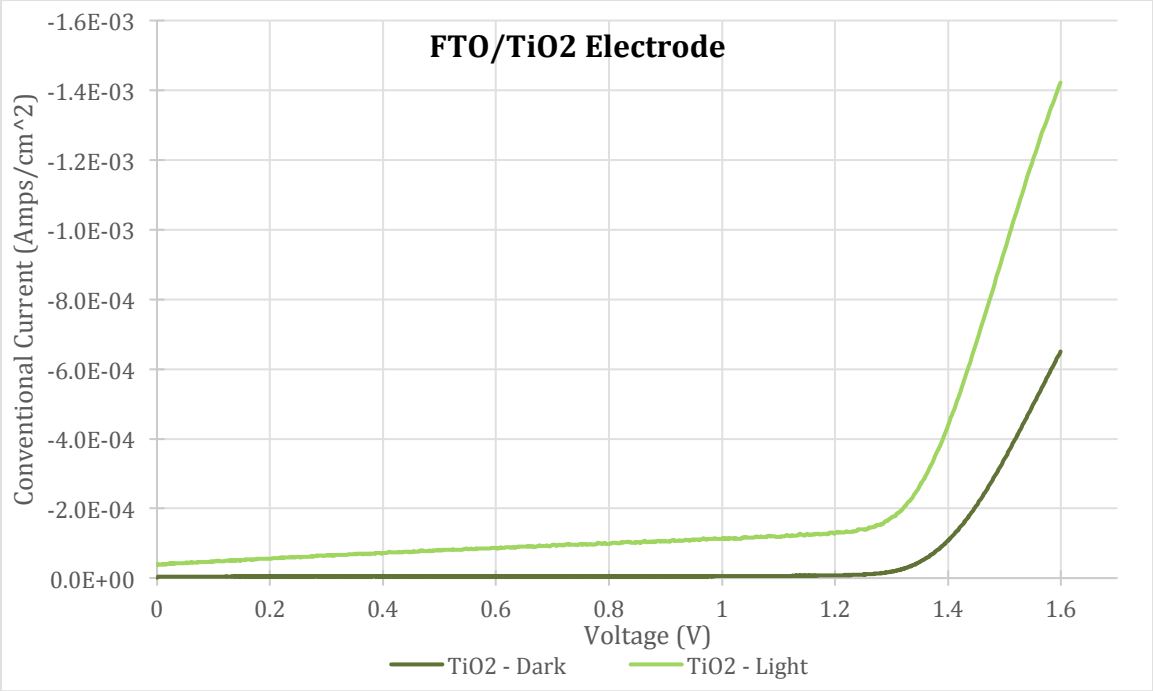

B.2 PEC Tests for $Bi[VO_4]_3$ Deposition Methods

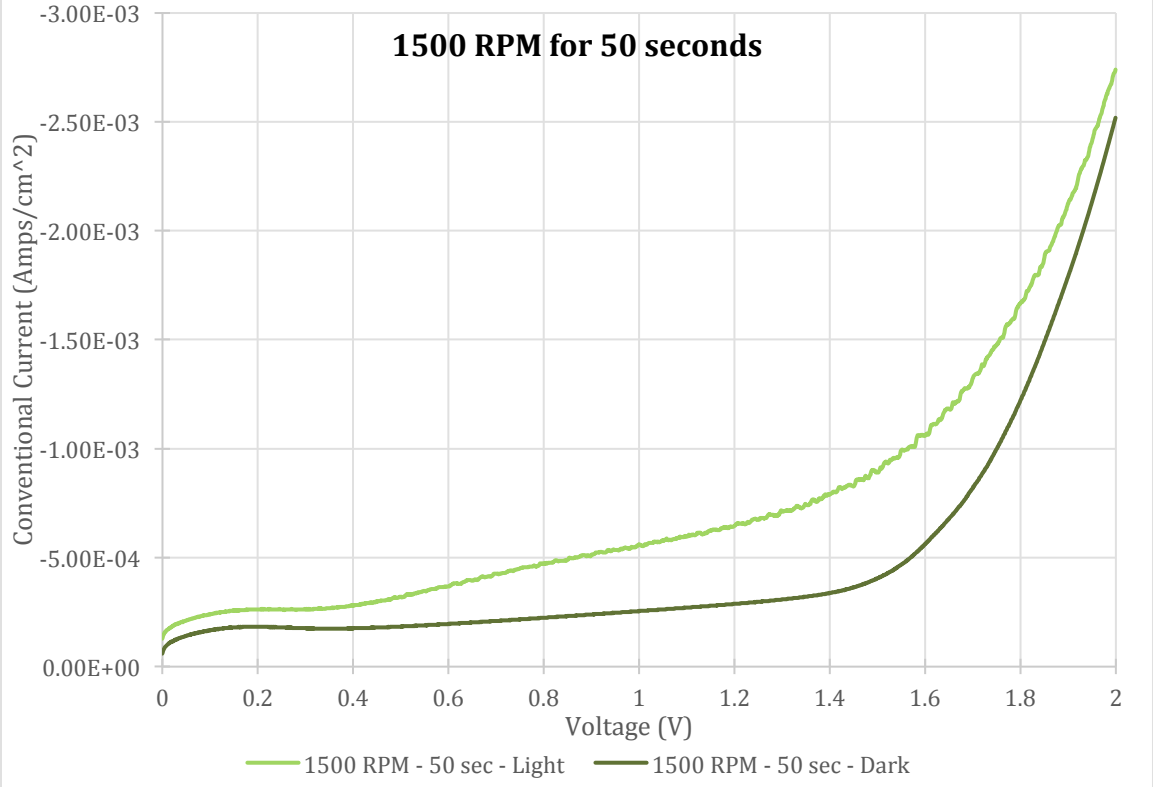

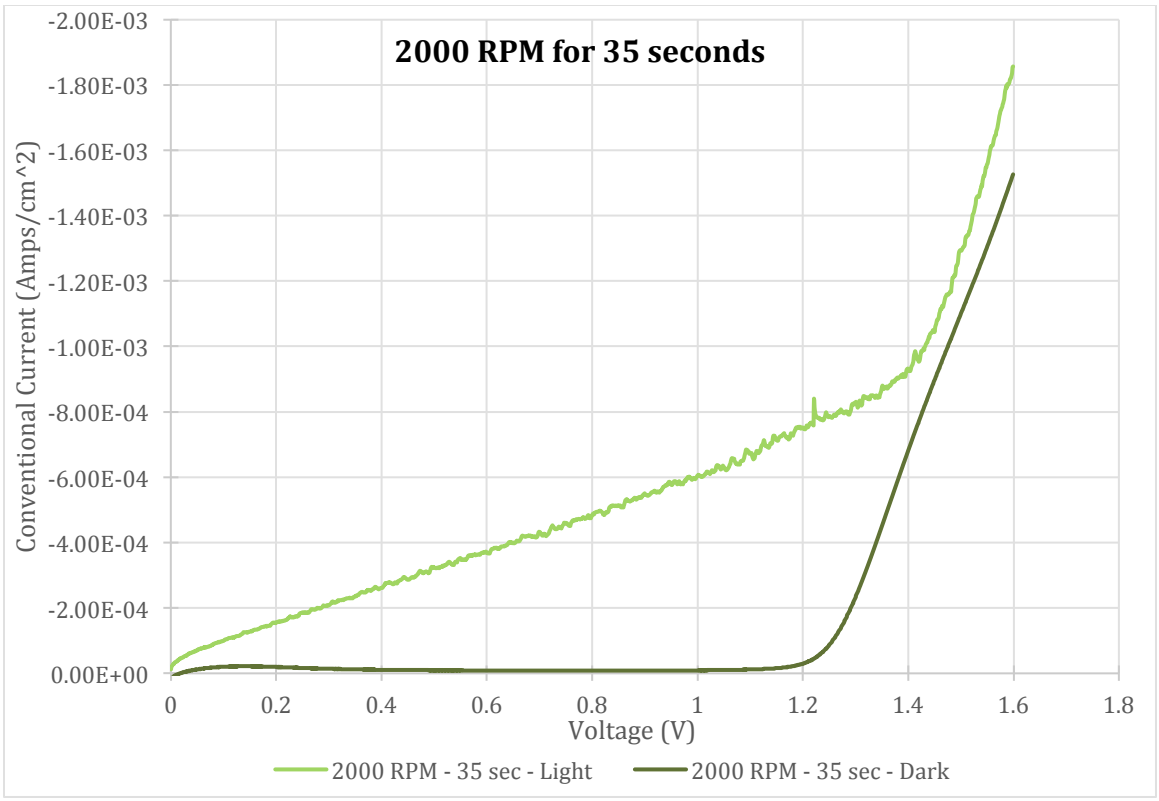
2000 RPM for 35 seconds
Conventional Current (Amps/cm^2)
-2.00E-03
-1.80E-03
-1.60E-03
-1.40E-03
-1.20E-03
-1.00E-03
-8.00E-04
-6.00E-04
-4.00E-04
-2.00E-04
0.00E+00
0
0.2
0.4
0.6
0.8
1
1.2
1.4
1.6
1.8
Voltage (V)
2000 RPM - 35 sec - Light
2000 RPM - 35 sec - Dark

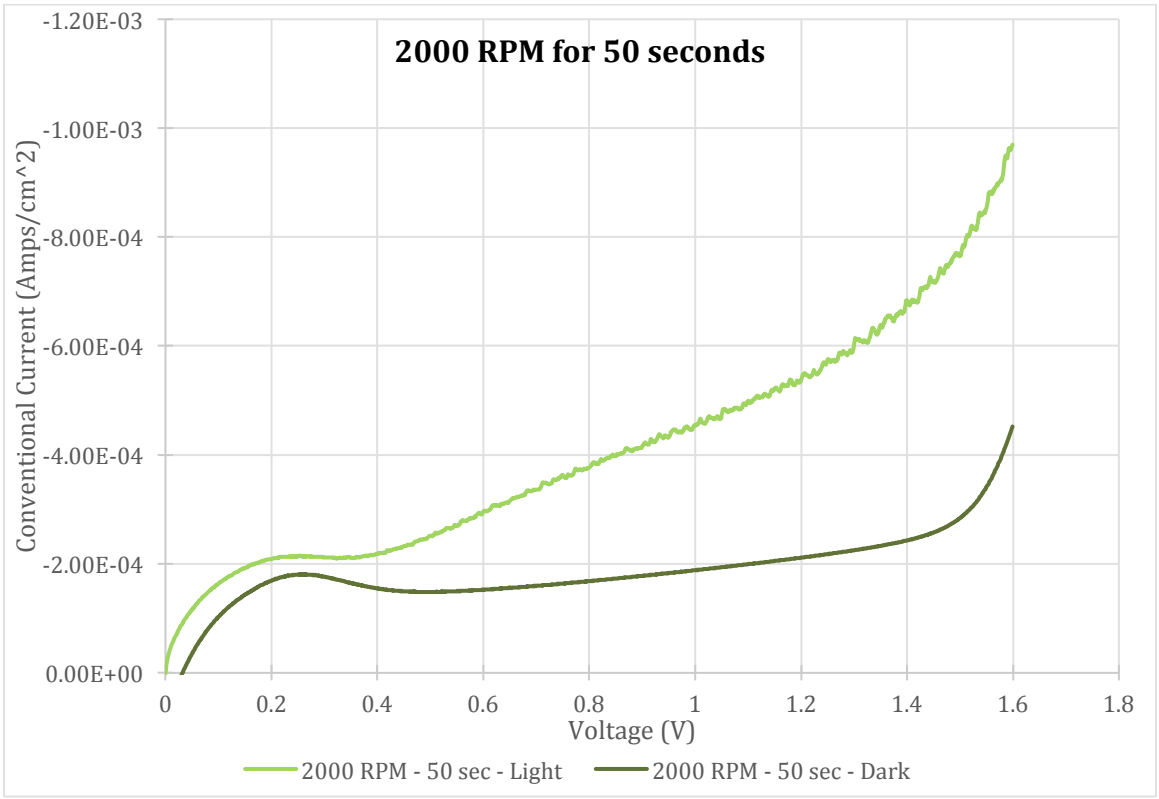
2000 RPM for 50 seconds
Conventional Current (Amps/cm^2)
-1.20E-03
-1.00E-03
-8.00E-04
-6.00E-04
-4.00E-04
-2.00E-04
0.00E+00
0
0.2
0.4
0.6
0.8
1
1.2
1.4
1.6
1.8
Voltage (V)
2000 RPM - 50 sec - Light
2000 RPM - 50 sec - Dark

B.3 PEC Tests for Cobalt Deposition

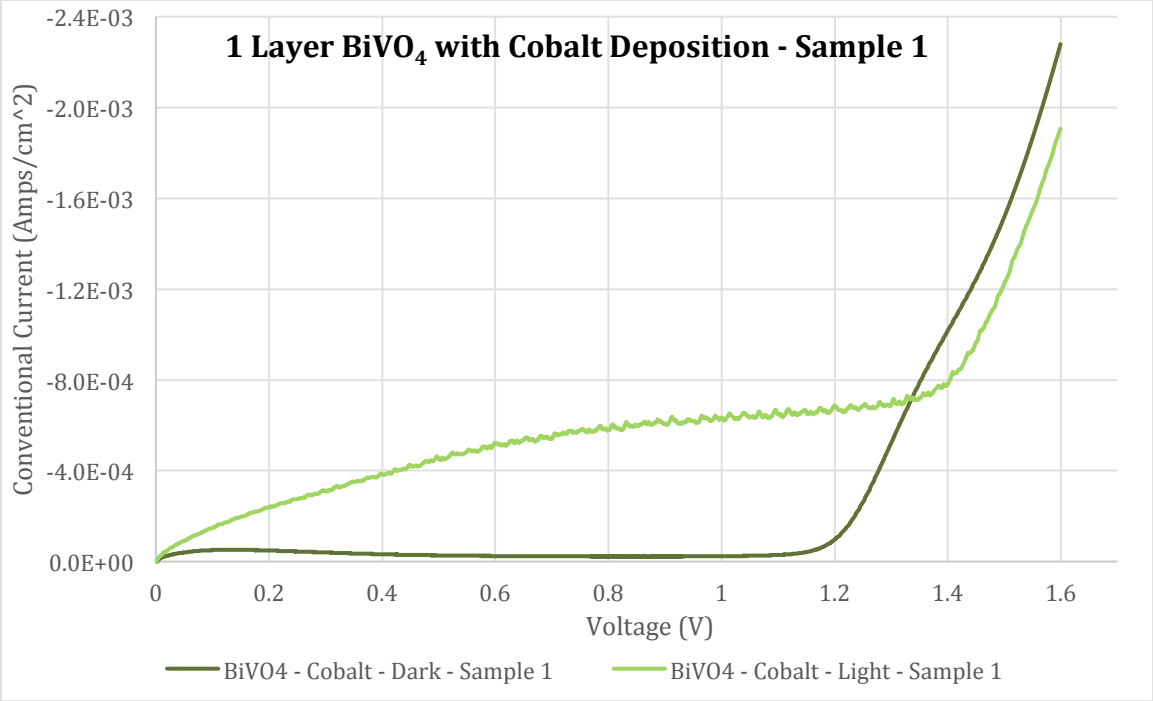

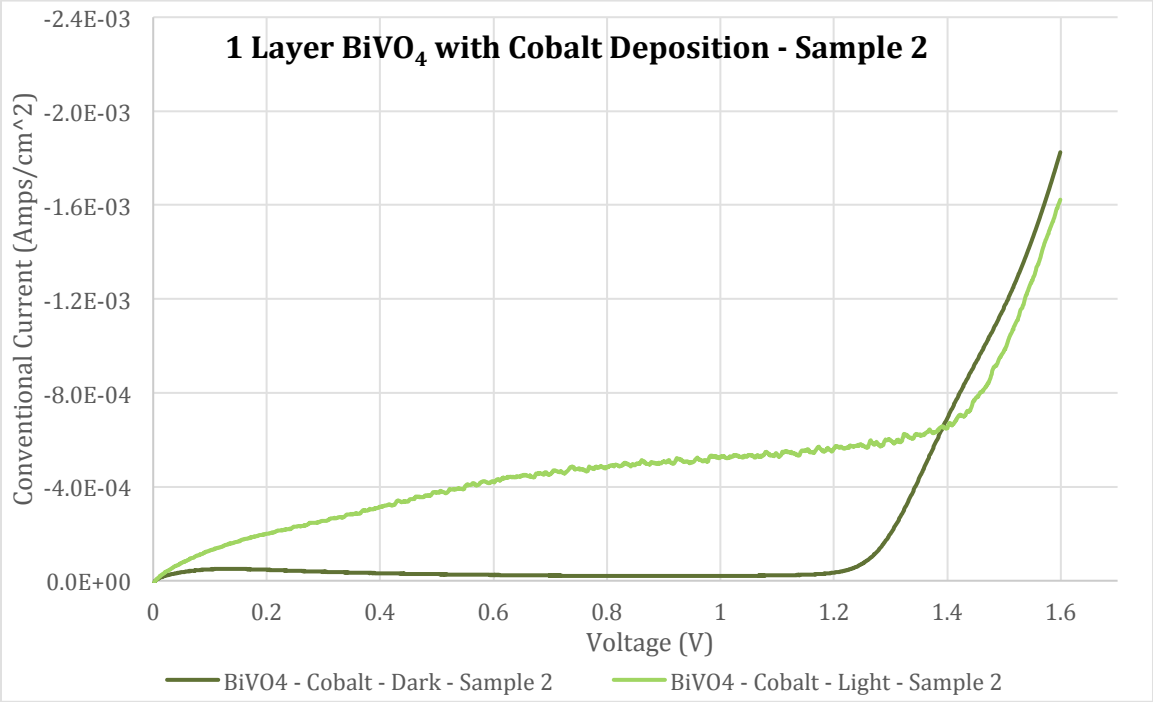

B.4 PEC Tests for Number of $Bi[VO_4]_3$ Layers

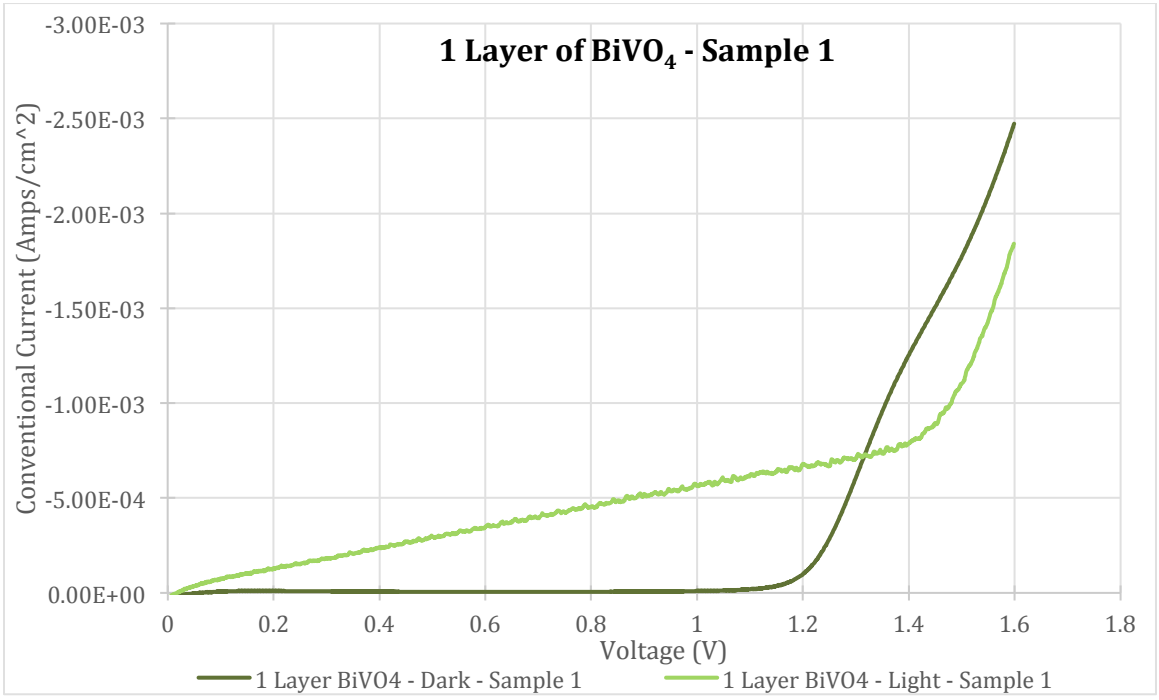

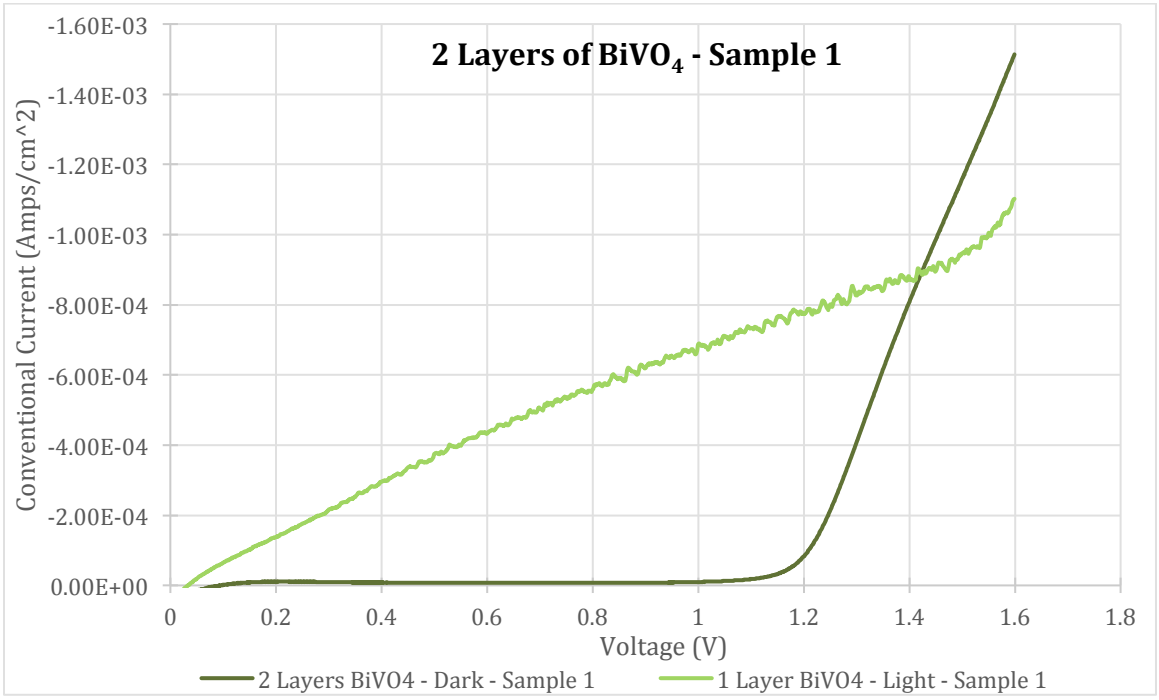

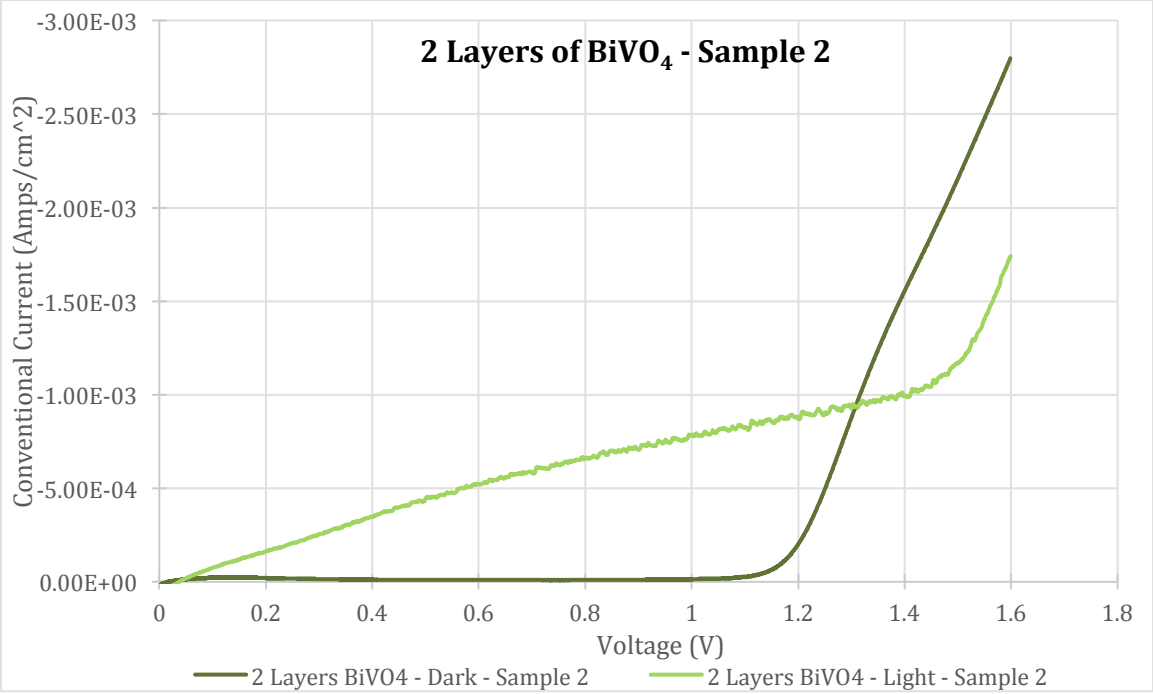
2 Layers of BiVO4 - Sample 2
Conventional Current (Amps/cm^2)
-3.00E-03
-2.50E-03
-2.00E-03
-1.50E-03
-1.00E-03
-5.00E-04
0.00E+00
0
0.2
0.4
0.6
0.8
1
1.2
1.4
1.6
1.8
Voltage (V)
2 Layers BiVO4 - Dark - Sample 2
2 Layers BiVO4 - Light - Sample 2

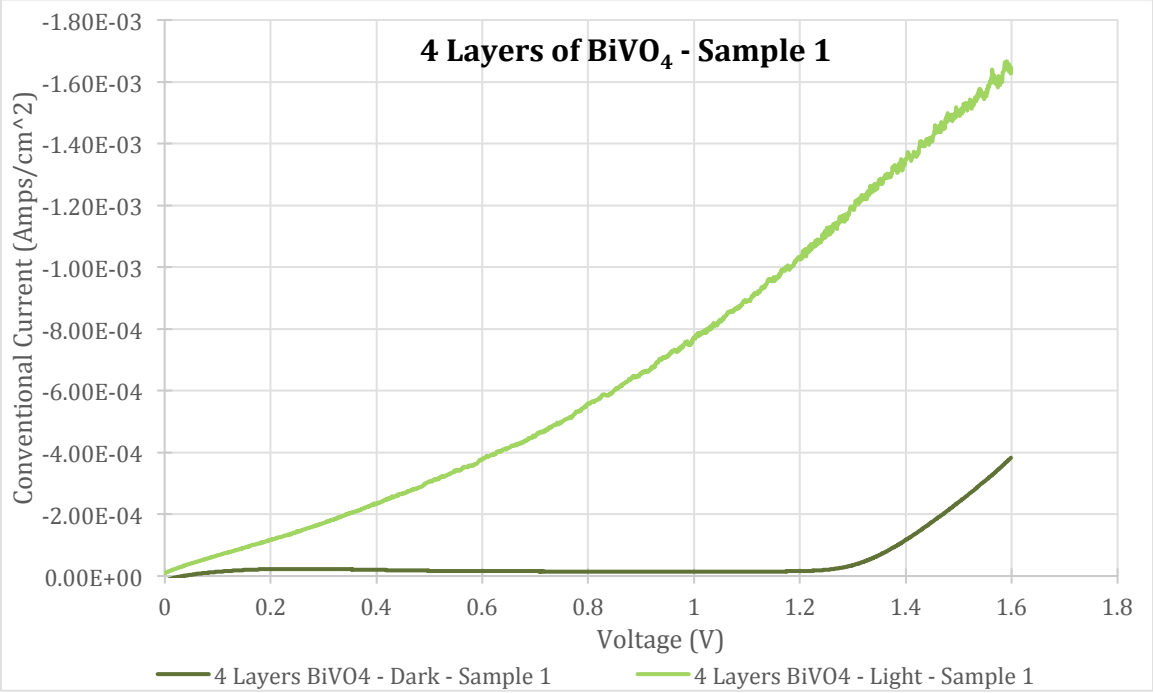
4 Layers of BiVO4 - Sample 1
Conventional Current (Amps/cm^2)
-1.80E-03
-1.60E-03
-1.40E-03
-1.20E-03
-1.00E-03
-8.00E-04
-6.00E-04
-4.00E-04
-2.00E-04
0.00E+00
0
0.2
0.4
0.6
0.8
1
1.2
1.4
1.6
1.8
Voltage (V)
4 Layers BiVO4 - Dark - Sample 1
4 Layers BiVO4 - Light - Sample 1

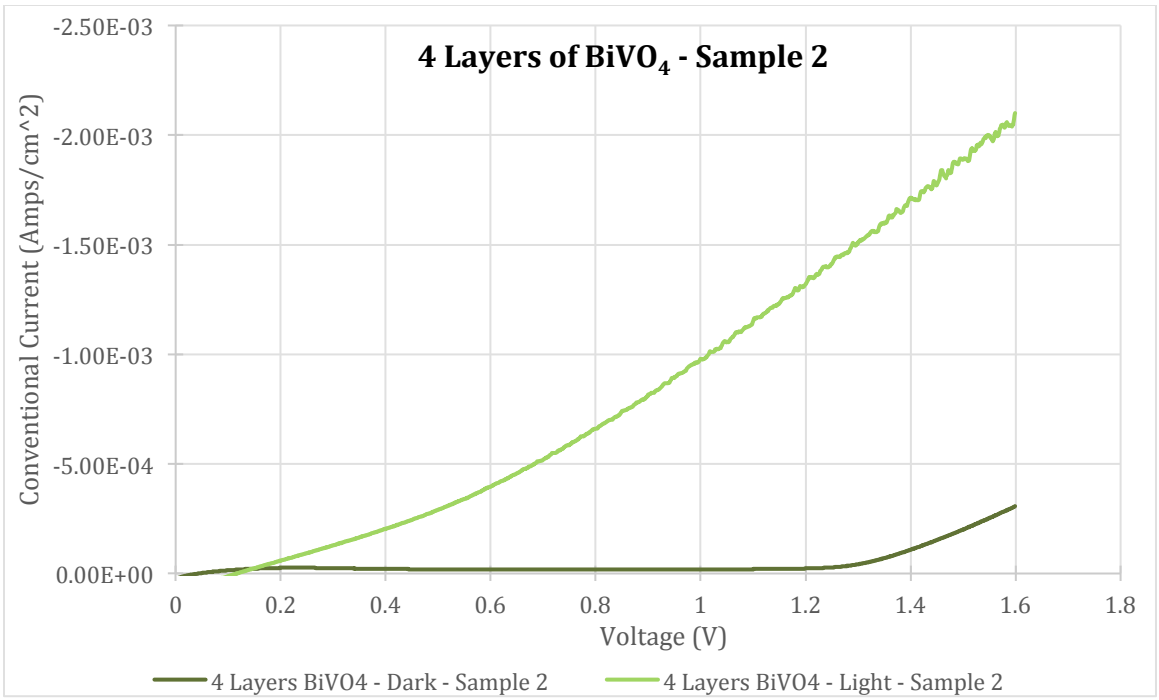
4 Layers of BiVO4 - Sample 2
Conventional Current (Amps/cm^2)
-2.50E-03
-2.00E-03
-1.50E-03
-1.00E-03
-5.00E-04
0.00E+00
0
0.2
0.4
0.6
0.8
1
1.2
1.4
1.6
1.8
Voltage (V)
4 Layers BiVO4 - Dark - Sample 2
4 Layers BiVO4 - Light - Sample 2

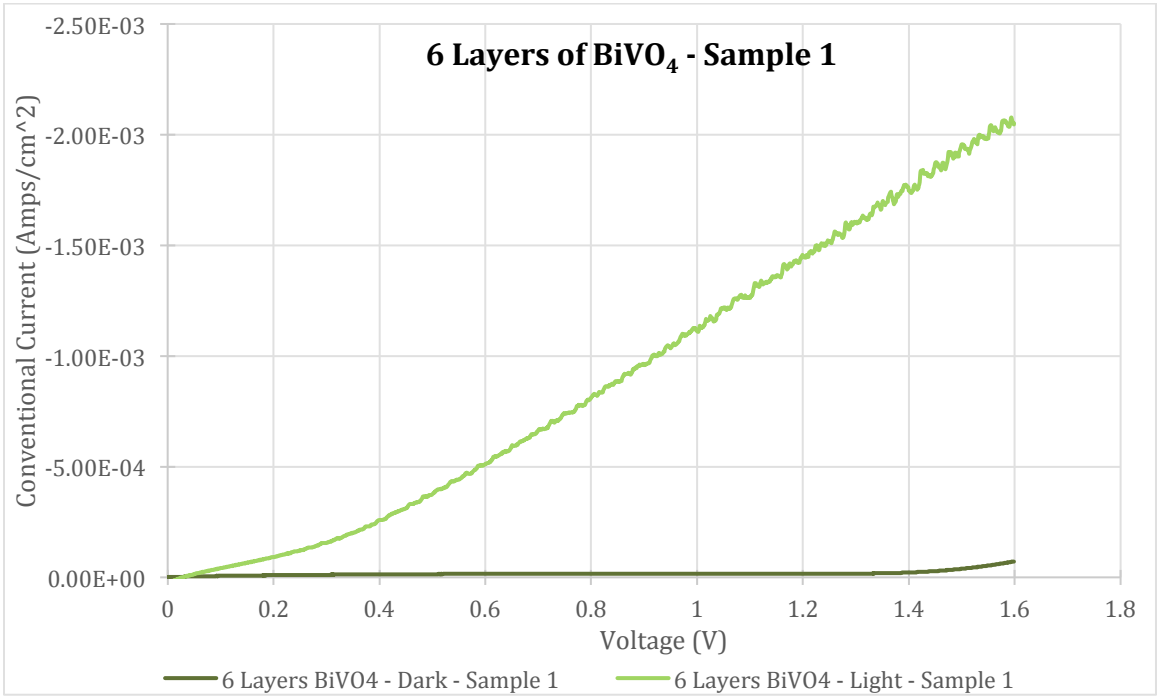
6 Layers of BiVO4 - Sample 1
Conventional Current (Amps/cm^2)
-2.50E-03
-2.00E-03
-1.50E-03
-1.00E-03
-5.00E-04
0.00E+00
0
0.2
0.4
0.6
0.8
1
1.2
1.4
1.6
1.8
Voltage (V)
6 Layers BiVO4 - Dark - Sample 1
6 Layers BiVO4 - Light - Sample 1

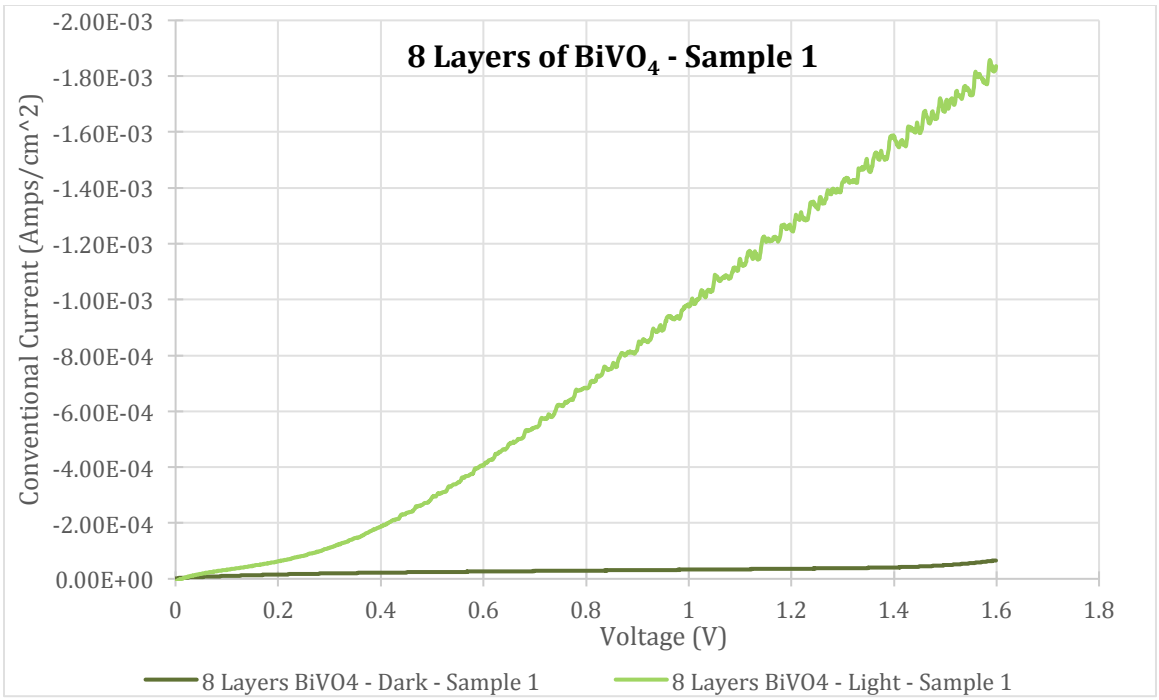
8 Layers of BiVO4 - Sample 1
Conventional Current (Amps/cm^2)
-2.00E-03
-1.80E-03
-1.60E-03
-1.40E-03
-1.20E-03
-1.00E-03
-8.00E-04
-6.00E-04
-4.00E-04
-2.00E-04
0.00E+00
0
0.2
0.4
0.6
0.8
1
1.2
1.4
1.6
1.8
Voltage (V)
8 Layers BiVO4 - Dark - Sample 1
8 Layers BiVO4 - Light - Sample 1

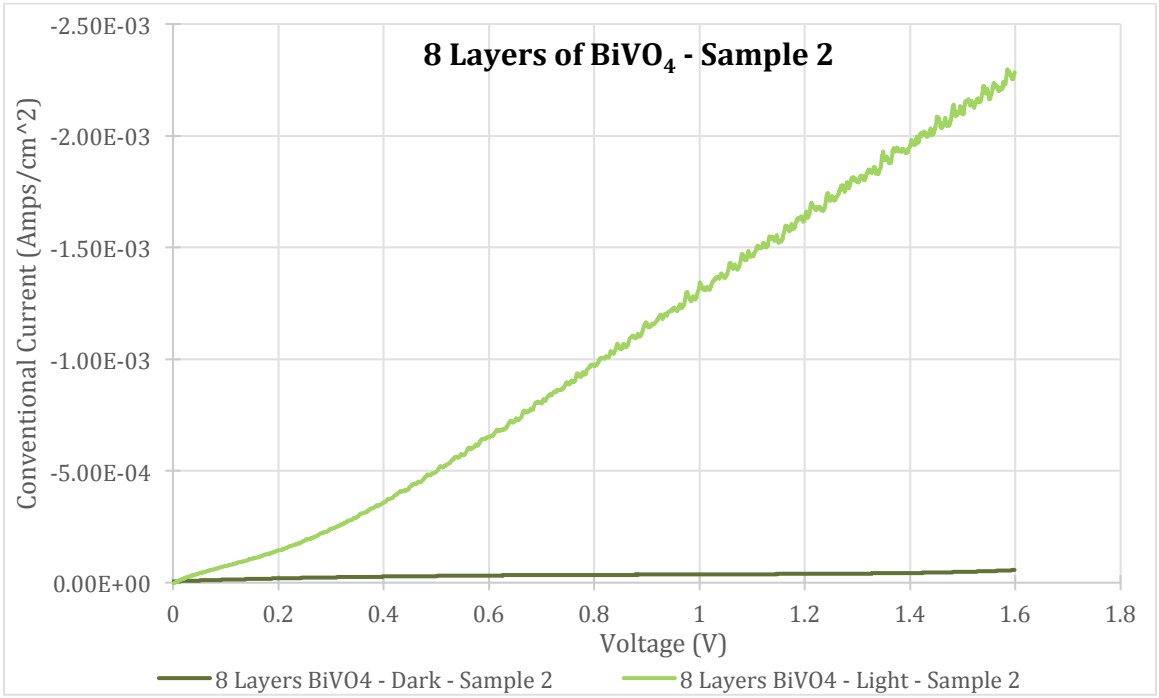
8 Layers of BiVO4 - Sample 2
Conventional Current (Amps/cm^2)
-2.50E-03
-2.00E-03
-1.50E-03
-1.00E-03
-5.00E-04
0.00E+00
0
0.2
0.4
0.6
0.8
1
1.2
1.4
1.6
1.8
Voltage (V)
8 Layers BiVO4 - Dark - Sample 2
8 Layers BiVO4 - Light - Sample 2

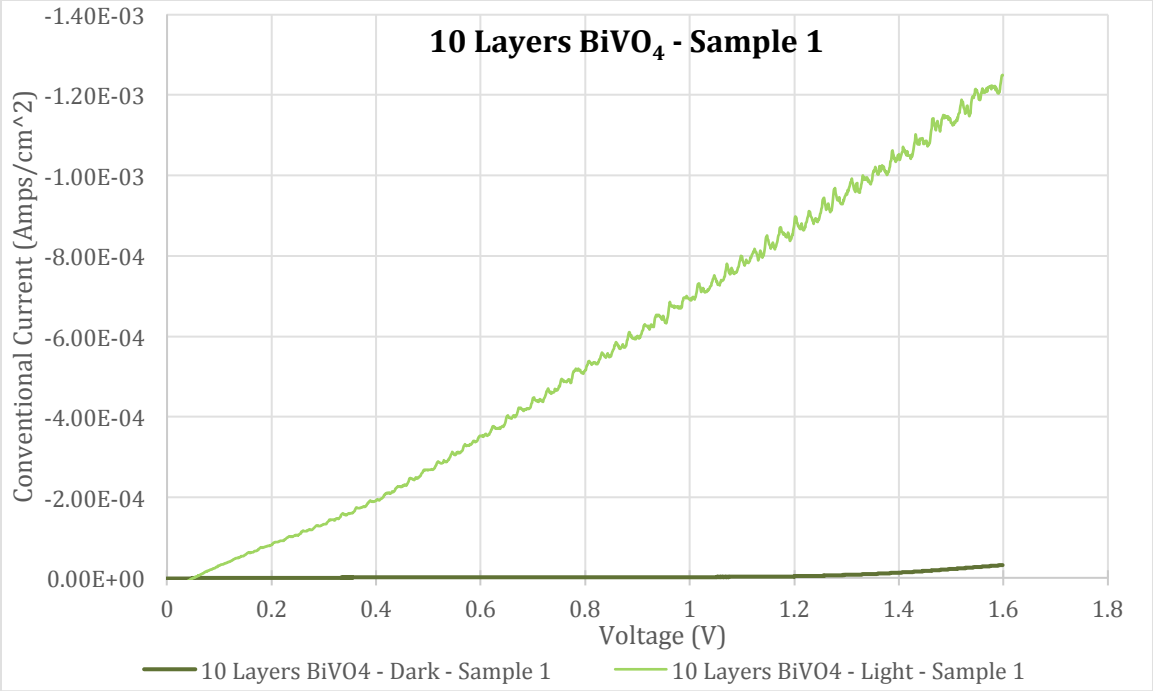
10 Layers BiVO4 - Sample 1
Conventional Current (Amps/cm^2)
-1.40E-03
-1.20E-03
-1.00E-03
-8.00E-04
-6.00E-04
-4.00E-04
-2.00E-04
0.00E+00
0
0.2
0.4
0.6
0.8
1
1.2
1.4
1.6
1.8
Voltage (V)
10 Layers BiVO4 - Dark - Sample 1
10 Layers BiVO4 - Light - Sample 1

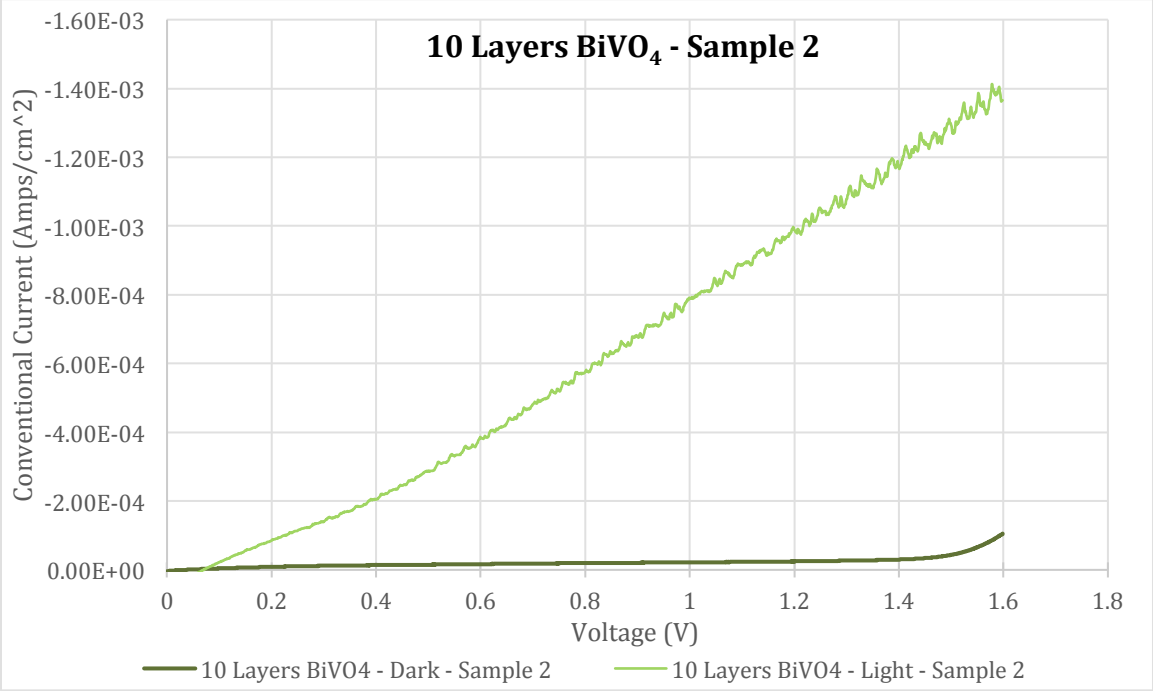
10 Layers BiVO4 - Sample 2
Conventional Current (Amps/cm^2)
-1.60E-03
-1.40E-03
-1.20E-03
-1.00E-03
-8.00E-04
-6.00E-04
-4.00E-04
-2.00E-04
0.00E+00
0
0.2
0.4
0.6
0.8
1
1.2
1.4
1.6
1.8
Voltage (V)
10 Layers BiVO4 - Dark - Sample 2
10 Layers BiVO4 - Light - Sample 2

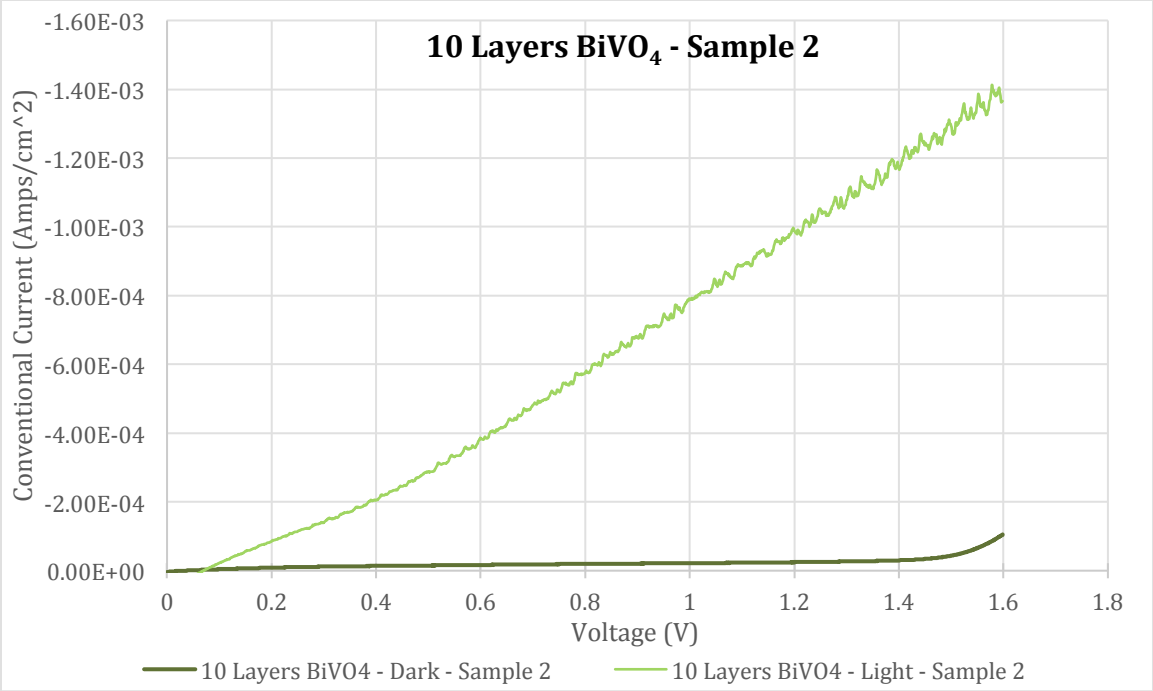
10 Layers BiVO4 - Sample 2
Conventional Current (Amps/cm^2)
-1.60E-03
-1.40E-03
-1.20E-03
-1.00E-03
-8.00E-04
-6.00E-04
-4.00E-04
-2.00E-04
0.00E+00
0
0.2
0.4
0.6
0.8
1
1.2
1.4
1.6
1.8
Voltage (V)
10 Layers BiVO4 - Dark - Sample 2
10 Layers BiVO4 - Light - Sample 2